

Modeling of Dolichol Mass Spectra Isotopic Envelopes as a Tool to Monitor Isoprenoid Biosynthesis^{1[OPEN]}

Adam Jozwiak², Agata Lipko, Magdalena Kania, Witold Danikiewicz, Liliana Surmacz, Agnieszka Witek, Jacek Wojcik, Konrad Zdanowski, Cezary Pączkowski, Tadeusz Chojnacki, Jarosław Poznanski*, and Ewa Swieżewska*

Institute of Biochemistry and Biophysics, Polish Academy of Sciences, 02-106 Warsaw, Poland (A.J., A.L., L.S., A.W., J.W., K.Z., T.C., J.P., E.S.); Institute of Organic Chemistry, Polish Academy of Sciences, 01-224 Warsaw, Poland (M.K., W.D.); Institute of Chemistry, University of Natural Sciences and Humanities, 08-110 Siedlce, Poland (K.Z.); and Department of Plant Biochemistry, Faculty of Biology, University of Warsaw, 02-096 Warsaw, Poland (C.P.)

ORCID IDs: 0000-0002-7666-7747 (A.J.); 0000-0002-4054-610X (A.L.); 0000-0003-0484-2689 (W.D.); 0000-0002-9517-1608 (L.S.); 0000-0002-3439-8948 (E.S.).

The cooperation of the mevalonate (MVA) and methylerythritol phosphate (MEP) pathways, operating in parallel in plants to generate isoprenoid precursors, has been studied extensively. Elucidation of the isoprenoid metabolic pathways is indispensable for the rational design of plant and microbial systems for the production of industrially valuable terpenoids. Here, we describe a new method, based on numerical modeling of mass spectra of metabolically labeled dolichols (Dols), designed to quantitatively follow the cooperation of MVA and MEP reprogrammed upon osmotic stress (sorbitol treatment) in *Arabidopsis thaliana*. The contribution of the MEP pathway increased significantly (reaching 100%) exclusively for the dominating Dols, while for long-chain Dols, the relative input of the MEP and MVA pathways remained unchanged, suggesting divergent sites of synthesis for dominating and long-chain Dols. The analysis of numerically modeled Dol mass spectra is a novel method to follow modulation of the concomitant activity of isoprenoid-generating pathways in plant cells; additionally, it suggests an exchange of isoprenoid intermediates between plastids and peroxisomes.

Isopentenyl diphosphate (IPP), the building block of isoprenoids, the most numerous class of secondary metabolites, is derived in plants from two pathways operating in parallel: the cytoplasmic mevalonate (MVA) and the plastidic methylerythritol phosphate (MEP) pathways (Rohmer, 1999; Pulido et al., 2012).

Analysis of over 130 isoprenoids has shown that, in angiosperms under standard growth conditions, carotenoids and chlorophyll phytyl chains on the one hand and phytosterols on the other are made nearly exclusively via a single pathway (MEP and MVA, respectively), while numerous other isoprenoids, including dolichols (Dols; Skorupinska-Tudek et al., 2008), are of mixed origin (Hemmerlin et al., 2012).

¹ This work was supported by the National Science Centre of Poland (grant nos. UMO-2012/07/B/NZ3/02437 and UMO-2012/06/M/NZ3/00155 to E.S. and grant no. UMO-2011/03/B/NZ1/00568 to L.S.) and the Foundation for Polish Science (grant no. MPD/2009-3/2 to A.L.) in a project cofinanced from the European Union Regional Development Fund.

² Present address: Department of Plant and Environmental Sciences, Weizmann Institute of Science, Rehovot 7610001, Israel.

* Address correspondence to jarek@ibb.waw.pl or ewas@ibb.waw.pl.

The author responsible for distribution of materials integral to the findings presented in this article in accordance with the policy described in the Instructions for Authors (www.plantphysiol.org) is: Ewa Swieżewska (ewas@ibb.waw.pl).

A.J., T.C., J.P., and E.S. designed experiments; A.J. was responsible for tissue culture, feeding experiments, lipid extraction, and purification; A.J. and A.L. synthesized pathway-specific precursors; T.C. contributed unique chemicals; M.K., W.D., J.W., and K.Z. performed structural analysis of dolichols; C.P. performed GC-MS analysis of phytosterols; A.J., L.S., and A.W. performed analysis of gene expression; A.J., A.L., J.P., and E.S. analyzed the data; A.J., J.P., and E.S. wrote the article.

^[OPEN] Articles can be viewed without a subscription.

www.plantphysiol.org/cgi/doi/10.1104/pp.17.00036

The cooperation of the two pathways (often called cross talk) is considered essential for plant adaptive responses to biotic and abiotic stresses. Consequently, their relative contributions to the formation of IPP are modulated, and the expression of particular genes of the MVA and MEP pathways is frequently correlated with stress (pathogen attack, elicitation, wounding, etc.; Hemmerlin et al., 2012) or plant development (Opitz et al., 2014). Interestingly, the effect of stress on the regulation of the MEP-MVA balance has so far been analyzed only qualitatively.

Several methodologies have been employed to unravel the relative contributions of the MVA and MEP pathways to isoprenoids, such as metabolic labeling with isotopically labeled precursors (stable isotopes or radioisotopes were used), followed by structural analysis of the product of interest or blockage of the pathway (chemical, with pathway-specific inhibitors, or genetic), followed by quantification of the isoprenoid intermediates and/or end products. The advantages

led to the conclusion that Prenyls of plant origin with a chain length within the range of five to nine and more than 16 isoprenoid residues as well as Prenyls isolated from bacteria belong to di-*trans*-structures (trivial name, betulaprenols), suggesting that farnesyl diphosphate (FPP) serves as their all-*trans*-initiator. The same type of structure (i.e. FPP-initiated biosynthesis) was found for Dols. Prenyls with a middle chain length (nine to 15 residues) represent tri-*trans*-compounds (trivial name, ficaprenols), indicating their origin from all-*trans*-geranylgeranyl diphosphate (Swiezewska and Danikiewicz, 2005).

The importance of Dol in the cell comes from the indispensable role of dolichyl phosphate as an obligate cofactor for protein glycosylation, a ubiquitous post-translational modification found in all domains of life (Schwarz and Aebi, 2011). The glycosylation of proteins is crucial for cell functioning, since it modulates protein folding and quality control, and is a prerequisite for diverse biological recognition events (Moremen et al., 2012). Furthermore, based on the considerably increased accumulation of polyisoprenoids in eukaryotic cells upon aging or pathological conditions, their role in cell adaptation to such conditions has been postulated too (Bergamini, 2003; Bajda et al., 2009).

The accumulation of diverse specialized metabolites, including isoprenoids, often is induced by abiotic or biotic stimuli (Sharma et al., 2013). In response to a changing environment, a specific gene expression program is activated and the plant metabolic network is reconfigured to maintain essential metabolism and to adjust to the new conditions.

In this study, a novel method to quantitatively analyze the cooperation of the MEP and MVA pathways was established using numerical models of the mass spectra of metabolically labeled Dols. It allowed us to follow the reorganization of isoprenoid metabolism upon osmotic stress and suggested a significantly increased contribution of the MEP pathway to Dol biosynthesis: upon the stress, practically all isoprene units of the dominating Dols (Dol-14 to Dol-16) originated from the MEP pathway, in contrast to control conditions, where only 11 or 12 units were of MEP origin. Conversely, the relative contributions of the MEP and MVA pathways to long Dols ($n > 17$) were unaltered upon osmotic stress (again, 11 or 12 units from the MEP pathway), suggesting a different, possibly peroxisomal, site of their biosynthesis. In a broader perspective, the methodology applied here can be used to analyze the effect of various stressors on the cooperation of the MEP and MVA pathways in plant cells.

RESULTS

Here, we describe the method to quantitatively analyze the contribution of the MEP and MVA pathways to the biosynthesis of selected isoprenoids in plant cells. The methodology employed here exemplifies the use of isotope tracing to define the metabolic pathway, and, in

general, such a strategy is widely employed in the field of isoprenoids. It is based on metabolic labeling with isotope-labeled general (Glc) and pathway-specific (MVA or deoxyxylulose [DX]) precursors followed by analysis of the structure of the compound of interest. In this report, a meta-analysis of mass spectra of metabolically labeled Dols was performed: numerical simulation of the shape of their isotopic envelope. Such an approach takes into account all the cationic forms of the Dol ions recorded in the spectrum (Figs. 2 and 3). Analysis of the mass spectrometry (MS) spectra of Dols metabolically labeled with uniformly labeled [$U\text{-}^{13}\text{C}_6$]Glc led to quantitative estimation of the general cellular effects due to sorbitol treatment (Fig. 5; Supplemental Fig. S3). However, to elucidate the contribution of the MEP and MVA pathways to Dol biosynthesis, spectra obtained after metabolic labeling with [$1\text{-}^{13}\text{C}$]Glc were analyzed (Fig. 7). Application of this metabolic precursor permits the differentiation of MEP- and MVA-derived isoprene units (two or three ^{13}C atoms get incorporated, respectively; Fig. 1B); consequently, the molecular ions of respective Dol are either lighter or heavier (MEP or MVA derived, respectively). Modeling of MS spectra led to quantification of the contribution of the MEP and MVA pathways (Table II).

Dol Metabolism upon Osmotic Stress: Biochemical Analysis

To optimize the experimental conditions, the effects of various stressors on the levels and spectra of Dols in Arabidopsis hairy root culture were analyzed. The content of Dol in roots treated with sorbitol (0.2–0.5 M) increased compared with the control (Fig. 1) and their composition was modified; namely, the ratio of dominating to long-chain Dols increased upon most of the treatments tested (e.g. 5-fold in 0.3 M sorbitol; Table I), suggesting different roles of these two Dol subgroups in cell functioning. Furthermore, sorbitol caused diverse changes in the expression of CPT-encoding genes (Fig. 1); namely, the expression of *CPT3*, *CPT6*, and *CPT7* was induced while that of *CPT1*, *CPT2*, and *CPT9* was reduced considerably. Interestingly, a microarray analysis (eFP Browser; <http://bar.utoronto.ca/efp/cgi-bin/efpWeb.cgi>) also revealed enhanced expression of *CPT3* and *CPT6* upon osmotic stress. The changing ratio of Dol families and the contrasting responses of different CPT genes in response to osmotic stress suggested that at least three CPTs take part in Dol biosynthesis. Since CPT6 produces shorter prenyl alcohols (Kera et al., 2012; Surmacz et al., 2014), CPT3 and/or CPT7 might operate to synthesize dominating Dols. Moreover, out of six CPTs expressed in Arabidopsis roots, CPT3 seems the most similar to the yeast Rer2 CPT, synthesizing a family of Dols with Dol-16 dominating (Fig. 1). At the same time, one of the stress-nonresponsive CPTs (CPT1, CPT2, or CPT9) might be involved in the synthesis of long-chain Dols, because their accumulation is not induced by stress in Arabidopsis hairy roots.

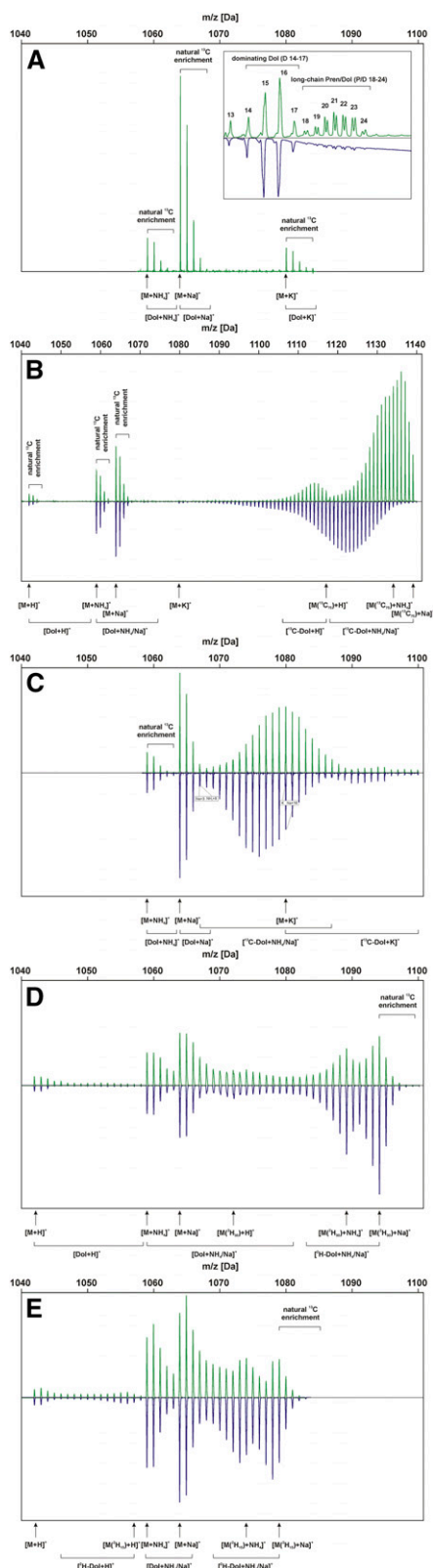


Figure 2. Mass spectra of Dol-15 metabolically labeled from various precursors applied in the absence (green trace; control) or presence (blue trace) of sorbitol. A, Native Dol-15. The inset presents UV spectra of polyisoprenoid mixtures isolated from roots grown in the absence or

These tempting suppositions, however, need experimental proofs. To analyze whether the effect of sorbitol on Dol accumulation is specific, the effects of oxidative agents and heavy metal salt (CdCl_2) were elucidated in parallel (Table I), and it was found that, apart from sorbitol, these abiotic stressors also increased Dol accumulation. Conversely, the expression pattern of CPTs was treatment specific (Supplemental Figs. S1 and S2), suggesting dedicated roles of individual CPTs in plant responses to different stresses and implying a role of reactive oxygen species (ROS) signaling in Dol generation. Analysis of the content of Prens, α -unsaturated counterparts accompanying Dols in *Arabidopsis* hairy roots (Jozwiak et al., 2013), performed in parallel, revealed a modest decrease of their total content with the concomitant increase of Dols upon sorbitol treatment (Fig. 1). Interestingly, similar to Dols, modulation of the Pren composition was noted too; namely, fraction containing Pren-15 to Pren-17 was increased considerably upon these conditions (Table I); since Pren-15 to Pren-17 serve as immediate substrates for polyprenol reductase (PPRD) to synthesize the respective Dols, this observation again points to the important cellular role of dominating Dols. Accordingly, a mild increase in the level of *PPRD2* mRNA (Fig. 1F), the main PPRD isoform responsible for the conversion of Prens to Dol in *Arabidopsis* seedlings (Jozwiak et al., 2015), was observed.

In contrast to the Dols, the total content of phytoosterols did not change upon sorbitol treatment (Table I).

To test the effect of osmotic stress on the MEP and MVA pathways, the roots were fed either $[\text{U-}^{13}\text{C}_6]\text{Glc}$ or $[\text{1-}^{13}\text{C}]\text{Glc}$ in the absence or presence of 0.3 M sorbitol, and isolated polyisoprenoids were subjected to HPLC/electrospray ionization-mass spectrometry (ESI-MS) analysis (Fig. 2). The spectra obtained were then analyzed numerically (i.e. the shape of the theoretical isotopic envelope of isotopomers of each Dol- n was fitted with the experimental one).

presence of sorbitol (green or blue trace, respectively). Signals corresponding to the analyzed Dol families (dominating Dols and long-chain Dols) are indicated. B, Feeding $[\text{U-}^{13}\text{C}_6]\text{Glc}$. C, Feeding $[\text{1-}^{13}\text{C}]\text{Glc}$. D, Feeding $[\text{2H}_2]\text{DX}$. E, Feeding $[\text{2H}]\text{mevalonolactone}$ (MVL). M is the m/z of monoisotopic $[\text{12C}_{75}]\text{Dol-15}$. Brackets above the spectra indicate signals of $[\text{13C}]\text{Dol-15}$ isotopomers synthesized from precursors with natural ^{13}C abundance. In B and C, arrows indicate signals corresponding to monoisotopic $[\text{12C}_{75}]\text{Dol-15}$ and $[\text{13C}_{75}]\text{Dol-15}$ ions: protonated $[\text{M}+\text{H}]^+$ or $[\text{M}(\text{13C}_{75})+\text{H}]^+$, ammoniated $[\text{M}+\text{NH}_4]^+$ or $[\text{M}(\text{13C}_{75})+\text{NH}_4]^+$, sodiated $[\text{M}+\text{Na}]^+$ or $[\text{M}(\text{13C}_{75})+\text{Na}]^+$, and potassiated $[\text{M}+\text{K}]^+$ or $[\text{M}(\text{13C}_{75})+\text{K}]^+$. Brackets at bottom denote signals corresponding to ^{13}C -enriched Dols in the indicated cationic forms. In D and E, arrows indicate signals corresponding to monoisotopic $[\text{1H}]\text{Dol-15}$ and expected precursor-specific maximally deuterium-labeled Dol-15 ions: protonated $[\text{M}(\text{2H}_{30})+\text{H}]^+$ or $[\text{M}(\text{2H}_{15})+\text{H}]^+$, ammoniated $[\text{M}(\text{2H}_{30})+\text{NH}_4]^+$ or $[\text{M}(\text{2H}_{15})+\text{NH}_4]^+$, and sodiated $[\text{M}(\text{2H}_{30})+\text{Na}]^+$ or $[\text{M}(\text{2H}_{15})+\text{Na}]^+$. Brackets at bottom denote signals corresponding to ^2H -enriched Dols in the indicated cationic forms.

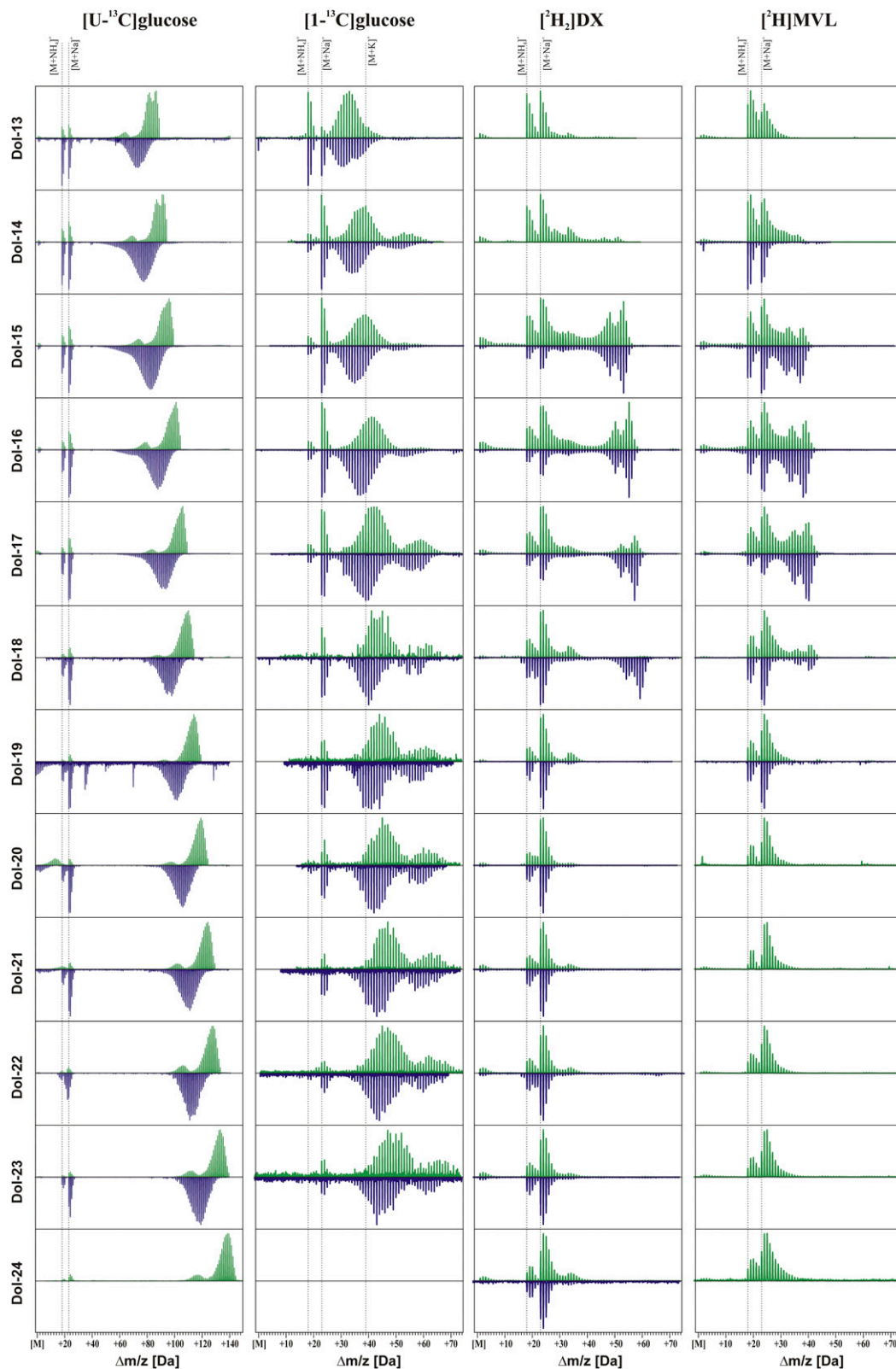


Figure 3. Mass spectra of Dols isolated from roots fed various metabolic precursors. $[U-^{13}C_6]Glc$, $[1-^{13}C]Glc$, $[^2H_2]DX$, or $[^2H]MVL$ were used in the absence or presence of sorbitol (green or blue traces, respectively). Dashed lines indicate the m/z of signals assigned to monoisotopic ions of ammoniated, sodiated, and potassiated $[^{12}C_{5n}]Dol-n$. Note that the m/z axis is adjusted to the value of the molecular mass (M) of monoisotopic $[^{12}C_{5n}]Dol-n$ for each Dol- n .

Table 1. Content of Dols, Prens, and phytosterols in *Arabidopsis* hairy roots exposed to various stress factors

Dol, Pren, and phytosterol content was estimated using HPLC/UV and gas chromatography-flame ionization detection (GC-FID); $n = 3$. Results significantly ($P < 0.05$) different from the control are indicated with asterisks. H_2O_2 , Hydrogen peroxide; MV, methyl viologen; *t*-BHP, *tert*-butyl hydroperoxide.

Stress		Dol Content	Fraction of Dominating Dols (Dol-14 to Dol-17) in Total Dol Mixture	Fraction of Prens (Pren-14 to Pren-17) in Total Pren Mixture	Phytosterol Content
		$\mu\text{g g}^{-1}$ fresh wt	%		mg g^{-1} fresh wt
Osmotic sorbitol (m)	Control	4.4 ± 0.6	67 ± 7	15 ± 1	2.1 ± 0.4
	0.2	4.9 ± 0.6	76 ± 9	22 ± 2	1.9 ± 0.3
	0.3	$6.4 \pm 0.6^*$	91 ± 8	36 ± 3	1.9 ± 0.5
	0.4	$6.9 \pm 0.4^*$	93 ± 9	35 ± 3	1.9 ± 0.7
	0.5	$6.5 \pm 0.1^*$	88 ± 5	38 ± 4	1.9 ± 0.6
Oxidative	Control	4.4 ± 0.2	66 ± 3	14 ± 2	2.0 ± 0.6
	1 mM H_2O_2	$5.3 \pm 0.3^*$	81 ± 4	23 ± 2	1.9 ± 0.2
	0.3 mM <i>t</i> -BHP	$5.8 \pm 0.6^*$	88 ± 5	26 ± 2	$5.2 \pm 0.4^*$
	1 μM MV	4.0 ± 0.2	61 ± 7	12 ± 1	$4.0 \pm 0.6^*$
CdCl_2 (μM)	Control	4.4 ± 0.5	67 ± 7	15 ± 2	2.0 ± 0.3
	25	$5.6 \pm 0.3^*$	86 ± 8	27 ± 2	2.3 ± 0.3
	50	$6.6 \pm 0.6^*$	91 ± 4	28 ± 2	2.0 ± 0.3

Elucidation of Dol Biosynthesis: Application of MS to Analyzing [^{13}C]Dols

To address the possible modulatory effect of osmotic stress on the cooperation of the MVA and MEP pathways, *Arabidopsis* hairy roots were metabolically fed either with [$U\text{-}^{13}\text{C}_6$]Glc or [$1\text{-}^{13}\text{C}$]Glc in the absence or presence of 0.3 M sorbitol, and isolated polyisoprenoids (Fig. 2A, inset) were subjected to HPLC/ESI-MS analysis. Careful inspection of the mass spectra of the [^{13}C]Dols revealed a complex pattern of signals (Figs. 2 and 3). The complexity of these mass spectra reflects the dispersion of the probability of formation of differentially labeled [^{13}C]Dol isotopomers/isotopologs (Skorupinska-Tudek et al., 2008). One should also note that, upon MS analysis, Dols form monovalent ions ($z = 1$); thus, the recorded m/z corresponds to the mass of the ion (Skorupinska-Tudek et al., 2003; Jozwiak et al., 2013). Moreover, the signal of each isotopomer (of a given m/z) in fact corresponds to various isotopologs (Dol ions containing the same number of ^{13}C atoms differently localized along the polyisoprenoid chain). Since this phenomenon was not analyzed here, the discrete isotopological structure of the MS spectrum will not be discussed further.

The spectra of native and metabolically labeled Dols (Figs. 2 and 3) isolated from roots grown in the control and osmotic stress conditions clearly revealed that, besides the $[\text{M}+\text{Na}]^+$ adducts identified earlier (Skorupinska-Tudek et al., 2008), also signals corresponding to $[\text{M}+\text{NH}_4]^+$ were noticed, and in some runs, $[\text{M}+\text{H}]^+$ or $[\text{M}+\text{K}]^+$ also were observed (Fig. 2 for Dol-15). Interestingly, among the two latter forms, protonated ions were more abundant for short-chain Dols, while potassiumated ions were more abundant for long-chain Dols (Fig. 3). Importantly, the isotopic profiles of all the types of adducts (i.e. their isotopic envelopes) reflected those observed for sodiated ions (Figs. 2 and 3). The observed complexity of the MS spectra recorded

in this report probably mirrored the technical conditions of the analysis: application of an instrument with particular parameters of the ion source and a high-sensitivity detector.

In the MS spectra of metabolically labeled Dols, native Dols, with natural ^{13}C enrichment ($\sim 1\%$), were found in addition to the [^{13}C]Dols formed due to the utilization of [^{13}C]Glc (Figs. 2 and 3). They originated from the inoculum of the *Arabidopsis* hairy roots used to initiate culture growth (Skorupinska-Tudek et al., 2008).

The same ratio of signal intensities of sodiated $[\text{M}+\text{Na}]^+$ versus ammoniated $[\text{M}+\text{NH}_4]^+$ ions was found for a given Dol- n species across all n values (Fig. 4), suggesting the reproducibility of the experimental conditions at the biological and analytical levels.

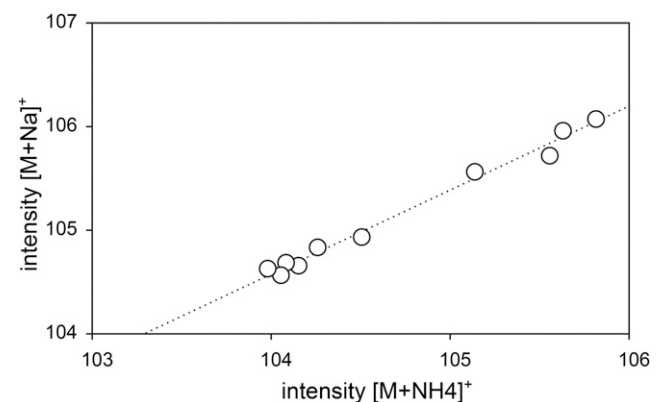


Figure 4. Correlation of signal intensities of cationic adducts, ammoniated $[\text{M}+\text{NH}_4]^+$ versus sodiated $[\text{M}+\text{Na}]^+$, for monoisotopic [$^{12}\text{C}_{5n}$]Dol- n ions of each Dol- n species (for explanation, see Fig. 2 for Dol-15). Shown are data obtained after labeling from [$U\text{-}^{13}\text{C}_6$]Glc. Note that such analysis was not possible for ^{13}C -enriched ammoniated and sodiated Dol- n isotopomers, since these distributions strongly overlapped (see Fig. 2).

Because of the cooccurrence of several types of Dol cationic adducts in the mass spectrum, the analysis of the isotopic envelope (the m/z value corresponding to its maximum) used in our previous study (Skorupinska-Tudek et al., 2008) could not be applied. Therefore, a new method based on numerical simulation of the shape of the isotopic envelope, taking into account all the cationic forms of the Dol ions, was used for further analysis.

Labeling with [U- $^{13}\text{C}_6$]Glc

The mass spectra of [^{13}C]Dols obtained from roots grown on [U- $^{13}\text{C}_6$]Glc as the sole carbon source comprised a complex set of signals (Fig. 3; for explanation, see Fig. 2). As expected, signals corresponding to the maximal m/z predicted for uniformly labeled [U- $^{13}\text{C}_{5n}$]Dol- n were identified, but numerous isotopic signals of hypolabeled [^{13}C]Dol isotopomers

were observed as well (Fig. 3). To investigate this phenomenon further, theoretical spectra of [^{13}C]Dols (i.e. theoretical isotopomer distributions) were calculated (see “Materials and Methods”, Eqs. 1 and 2).

In control conditions (roots grown in the medium devoid of sorbitol), for each Dol- n , the maximum of the isotopic envelope of the experimental spectrum for the [M+Na] $^+$ and [M+NH $_4$] $^+$ ions was located at an m/z lower than that calculated for the 99% ^{13}C isotopic abundance of the precursor [U- $^{13}\text{C}_6$]Glc (Fig. 5A for Dol-15). Therefore, we recalculated the spectra but with the assumption that the probability of ^{13}C incorporation in any given position of Dol- n was identical but lower than the declared 99% value (see “Materials and Methods”), corresponding to the isotopic abundance of the precursor Glc. This assumption took into account possible dilution of the exogenous ^{13}C -labeled substrate with endogenous Glc (with natural isotopic ^{13}C abundance of $\sim 1\%$). These theoretical spectra were optimized to achieve the best agreement with experimental

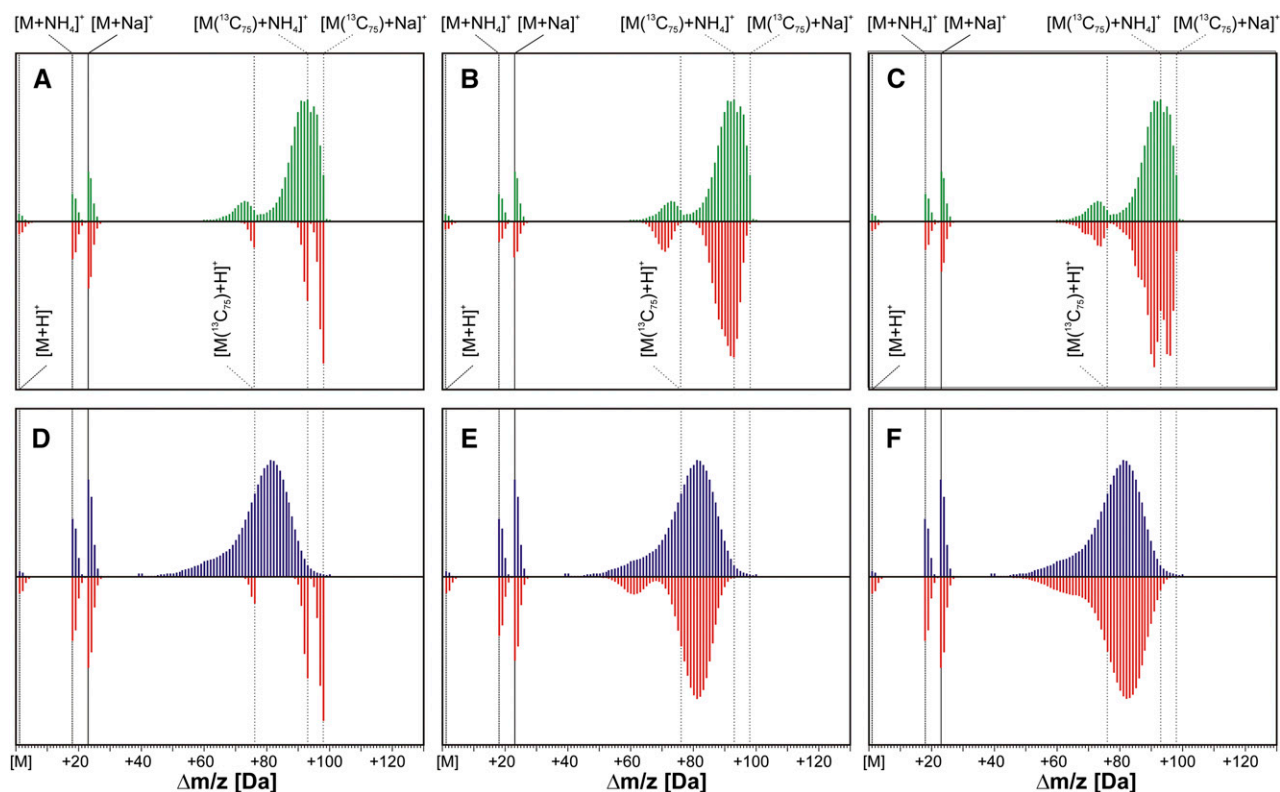


Figure 5. Comparison of theoretical and experimental mass spectra obtained for labeling of Dol-15 from [U- $^{13}\text{C}_6$]Glc in control and osmotic stress conditions. Three variants of the theoretical envelopes were calculated for both control (A–C) and osmotic stress (D–F) conditions. It was assumed that the isotopic enrichment of [^{13}C]Dol-15 was 99% (A and D), that is, it was synthesized from [U- $^{13}\text{C}_6$]Glc (99% ^{13}C isotopic abundance) as the sole source of carbon; and was $93.9 \pm 1\%$ (B) and $80.7 \pm 1.3\%$ (E) to account for some dilution with endogenous native Glc ($\sim 1\%$ ^{13}C isotopic abundance). Alternatively, labeling from [U- $^{13}\text{C}_6$]Glc together with an additional involvement of native IPP was considered: 96.1% [U- $^{13}\text{C}_6$]Glc and 2.8% native IPP (final isotopic enrichment of Dol-15 was $93.9 \pm 1\%$; C) or 87.4% [U- $^{13}\text{C}_6$]Glc and 8.5% native IPP (final isotopic enrichment of Dol-15 was $80.7 \pm 1.3\%$; F). Green and blue traces represent the experimental spectra recorded in control and osmotic stress conditions, respectively, while red traces represent the theoretical ones. Vertical lines indicate the m/z of the cationic, ammoniated ([M+NH $_4$] $^+$ and [M($^{13}\text{C}_{75}$)+NH $_4$] $^+$), and sodiated ([M+Na] $^+$ and [M($^{13}\text{C}_{75}$)+Na] $^+$) forms of the respective monoisotopic ions ([$^{13}\text{C}_{75}$]Dol-15, solid lines; [$^{13}\text{C}_{75}$]Dol-15, dotted lines).

ones (Fig. 5B for Dol-15; Supplemental Fig. S3 for Dol-*n*), and the best fit was obtained for the ^{13}C enrichment of $93.9\% \pm 1\%$ for all Dol-*n*. This value of the effective ^{13}C abundance was used further. The maxima of the isotopic envelopes of the theoretical mass spectra of Dol-*n* were in good agreement with the experimental ones but were slightly narrower than the latter, as shown for Dol-15 in Figure 5B (even more obvious for stress conditions; Fig. 5E). This discrepancy suggested that, besides native Glc, other native precursors (e.g. acetyl-CoA, trioses, or IPP) were incorporated into Dol (Fig. 5C).

In the presence of 0.3 M sorbitol, a striking shift of the mass spectrum of ^{13}C Dol toward lower *m/z* values compared with control conditions was observed (for Dol-15, compare Fig. 5, A and D). This shift was similar for all analyzed Dol-*n* (Fig. 3), suggesting a further dilution of the ^{13}C -labeled substrate/intermediate pool with their unlabeled counterparts upon sorbitol treatment. Theoretical spectra (Fig. 5E for ^{13}C Dol-15; Supplemental Fig. S3 for all Dol-*n*) calculated as above to fit the experimental ones revealed the effective ^{13}C enrichment of $80.7\% \pm 1.3\%$.

The differences between the mass spectra of ^{13}C Dols from sorbitol-treated versus control tissues (Fig. 3) were statistically significant for each Dol-*n* ($\alpha < 10^{-5}$), according to the Mann-Whitney test applied for pairs of corresponding cumulative distributions (Fig. 6). Importantly, similar values of the effective ^{13}C isotopic

abundance, $94.5\% \pm 1.3\%$ and $79\% \pm 1.2\%$ for the control and sorbitol-treated roots, respectively, were found for phytosterols synthesized in the presence of $[\text{U-}^{13}\text{C}_6]\text{Glc}$, confirming the universal nature of the observed metabolic effects of sorbitol (Fig. 8).

In summary, the $[\text{U-}^{13}\text{C}_6]\text{Glc}$ experiments led to the conclusion that sorbitol treatment decreases the ^{13}C enrichment of ^{13}C Dol from $93.9\% \pm 1\%$ to $80.7\% \pm 1.3\%$, most likely due to the mobilization of internal carbon sources, probably through starch hydrolysis upon osmotic stress (Krasensky and Jonak, 2012). Sorbitol itself is unlikely to serve as a carbon source, since its uptake from the medium is low and further decreased in the presence of Glc (Maurel et al., 2004). With the methodology applied here, the Dol labeling derived from $[\text{U-}^{13}\text{C}_6]\text{Glc}$ is biosynthetic route insensitive (MEP versus MVA), in contrast to the NMR-based approach (Bacher et al., 2016), but enables quantitative analysis of the cellular effects of sorbitol. To elucidate the contribution of the MEP and MVA pathways to Dol biosynthesis, $[\text{1-}^{13}\text{C}]\text{Glc}$ labeling followed by MS analysis was employed.

Labeling with $[\text{1-}^{13}\text{C}]\text{Glc}$

^{13}C atoms from $[\text{1-}^{13}\text{C}]\text{Glc}$ were incorporated into all analyzed Dols (Dol-13 to Dol-23; Fig. 3). Theoretical mass spectra of Dol-15 and Dol-20 synthesized from

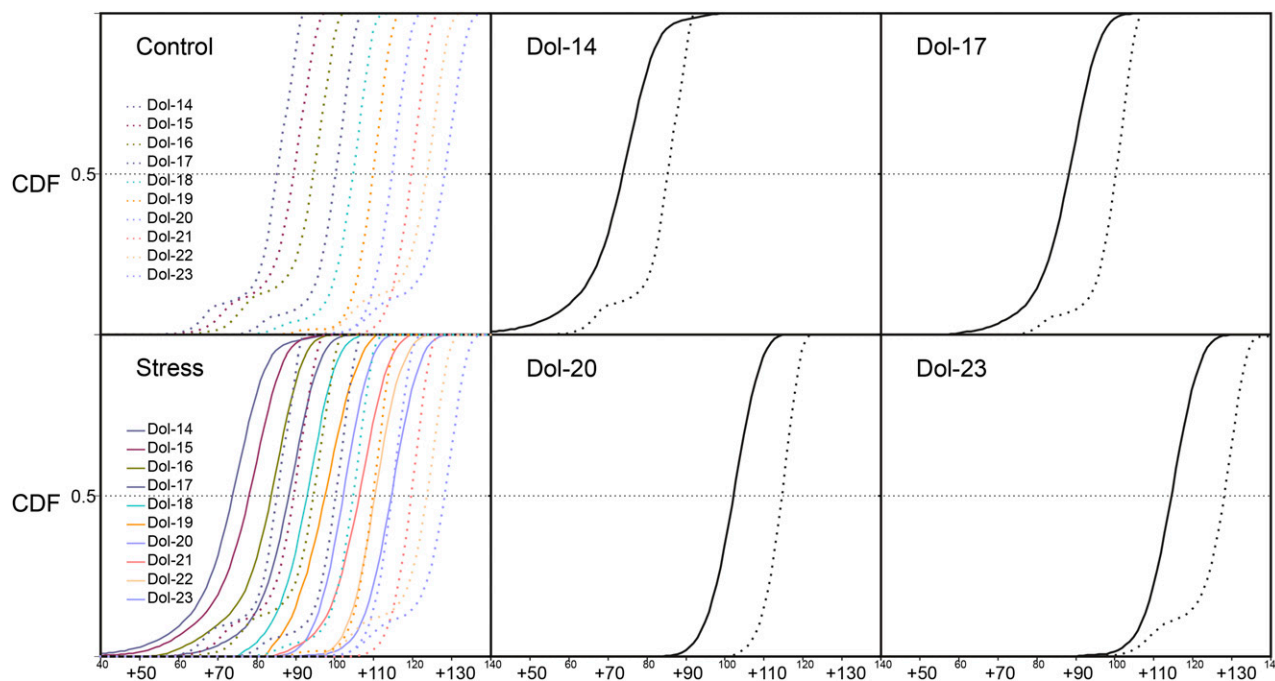


Figure 6. ^{13}C enrichment profiles of Dol-14 to Dol-23 metabolically labeled from $[\text{U-}^{13}\text{C}_6]\text{Glc}$ in the absence (dotted lines; control) or presence (solid lines) of sorbitol, represented as cumulative isotopomer distributions (CDF) directly derived from mass spectra. Overlaid CDFs are presented for all analyzed Dol-*n* as well as for selected Dol-14, Dol-17, Dol-20, and Dol-23. For each Dol-*n*, the differences between sorbitol-treated versus control roots are statistically significant ($\alpha < 10^{-5}$), according to the Mann-Whitney test applied for pairs of CDFs of respective Dol. Please note that the *m/z* axis is adjusted to the value of the molecular mass for each respective Dol-*n*.

[1-¹³C]Glc exclusively via either the MEP pathway (lighter isoprene units with two carbon atoms labeled; Fig. 7, A and A', respectively) or the MVA pathway (heavier units with three carbon atoms labeled; Fig. 7, B and B') were calculated (see "Materials and Methods," Eqs. 1 and 2) using the effective ¹³C abundances estimated (the expected labeling pattern is shown in Fig. 1B). For dominating Dols (shown for Dol-15; Fig. 7, A and B) upon control conditions, the experimentally recorded spectrum was located between the two theoretical mass spectra calculated for Dol synthesized via either the MEP or the MVA pathway (Fig. 7C), while upon stress, the experimental spectrum matched exactly the theoretical one modeled for Dol synthesized exclusively via the MEP pathway (Fig. 7D). However, for longer Dols, upon both incubation conditions, control (shown for Dol-20; Fig. 7, A' and B') and osmotic stress (Fig. 7, D' and E'), the recorded spectra located between the two theoretical distributions (Fig. 7, C' and F') and indicated, in accordance with our earlier results (Skorupinska-Tudek et al., 2008), a mixed biosynthetic origin of Dol. The same was observed for all other [¹³C]Dol-*n* (data not shown). Notably, in the presence of sorbitol, the experimental mass spectra of [¹³C]Dol were shifted toward lower *m/z* than those of the control (medium devoid of sorbitol; Fig. 3), similar to the results for labeling with [U-¹³C₆]Glc. This effect cannot be attributed to sorbitol-induced isotopic dilution or the loss of ¹³C atoms due to Glc catabolism via the oxidative pentose pathway, since these effects were already taken into account by adjusting the effective ¹³C isotopic abundance to 80.7%. However, the contribution of native IPP would result in an additional decrease of the ¹³C enrichment of Dol without, however, the broadening of the MS envelope that was observed for [U-¹³C₆]Glc labeling.

Cooperation of the MEP and MVA Pathways to Synthesize Dol

To quantitate the MEP and MVA input to Dol formation, theoretical isotopomer distributions showing reasonable agreement with the experimental ones were calculated for all Dols following Equation 3 in "Materials and Methods" (Fig. 7, C and F, for Dol-15, and C' and F', for Dol-20; Supplemental Fig. S3 for all Dols).

For control conditions, the number of isoprene units derived from the MEP pathway giving the best fit to the experimental spectra, n_{MEP} , is 11 or 12 for most of the Dol-*n* species. Consequently, the number of units derived from the MVA pathway, n_{MVA} , increases with the length of Dol from 3 (Dol-14) to 15 (Dol-23; Table II). This supports our hypothesis put forward earlier (Skorupinska-Tudek et al., 2008) that, regardless of the length of Dol, the MEP pathway mediates the synthesis of a common intermediate, while the number of MVA-derived units is variable. Therefore, it is the cytoplasmic MVA-derived IPP and cytoplasmic CPTs that are responsible for the observed breadth of the Dol family homologs. Interestingly, the contribution of the MEP

pathway seems considerably higher for *Arabidopsis* (11–12 isoprene units) than for *Coluria geoides* (6–8 isoprene units) roots (Skorupinska-Tudek et al., 2008), although, overall, the biosynthesis of Dol seems to be performed in a similar manner in these two plant species. The shortest species, Dol-13, seems to be an exception, since it contained only ~9 MEP-derived units, and this number was not increased upon stress (see below).

In the presence of sorbitol, the calculated n_{MEP} was 13 to 15 for Dol-14 to Dol-17 (the dominating Dols), suggesting a substantially increased contribution of the MEP pathway to their biosynthesis. In contrast, no such increase was observed for the longer Dols, Dol-18 to Dol-23 (Table II).

In accordance with the glycolytic catabolism of Glc with a stochastic mixing of triose pools, the ¹³C enrichment of Dols synthesized from [1-¹³C]Glc was close to one-half of the calculated effective ¹³C abundance in both control ($47.1\% \pm 0.9\%$ versus $93.9\% \pm 1\%$) and stress ($40.2\% \pm 0.8\%$ versus $80.7\% \pm 1.3\%$) conditions (Fig. 5, C and F, respectively).

Taken together, these data indicate a modulation of the relative activity of the isoprenoid-generating pathways in plant roots in response to osmotic stress, resulting in an increased contribution of the MEP pathway to the biosynthesis of dominating Dol, achieving virtually 100% for Dol-14 and Dol-15. Strikingly, the metabolic origins of both short-chain Dols (Dol-13) and long-chain Dols (Dol-18 to Dol-21) remain unaffected by sorbitol (Supplemental Fig. S4).

Sorbitol treatment also increased the contribution of the MEP pathway to phytosterol biosynthesis, but in this case, only qualitative analysis was possible (see below).

Application of Pathway-Specific Precursors

In order to elucidate further the effect of osmotic stress on the contribution of the two pathways to Dol biosynthesis, *Arabidopsis* roots were grown in medium supplemented with deuterated precursors specific to either the MEP pathway (DX) or the MVA pathway (MVL) in the absence or presence of 0.3 M sorbitol. Deuterated Dols were isolated and analyzed by MS. Consistent with the results of labeling with the general precursor Glc, the presence of various cationic derivatives (NH_4^+ , Na^+ , and K^+ as well as traces of H^+) resulted in a subtle structure of the spectra (Fig. 3). It should be kept in mind that the Dol molecules also contained ¹³C atoms due to the natural abundance of ¹³C (Fig. 2).

Labeling with [²H₂]DX

The presence of signals of a higher *m/z* in the mass spectra, in addition to those corresponding to native Dol molecules, clearly confirmed precursor incorporation (Fig. 3; two deuterium atoms per isoprene unit are

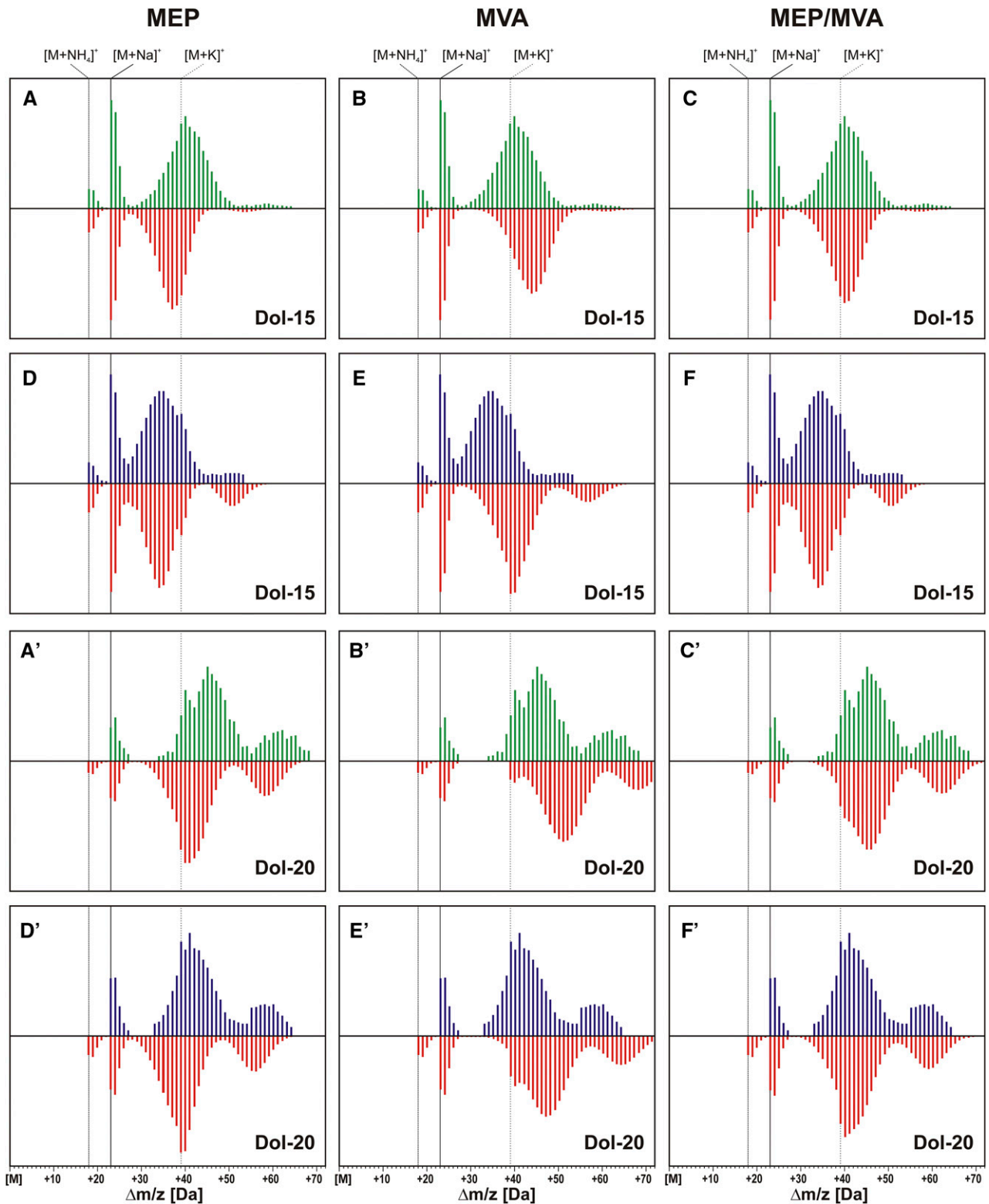


Figure 7. Comparison of theoretical and experimental mass spectra obtained for labeling of Dol-15 and Dol-20 from $[1-^{13}C]Glc$ in control and osmotic stress conditions. Three variants of the theoretical spectra were calculated for both control (A–C and A'–C') for Dol-15 and Dol-20, respectively) and osmotic stress (D–F and D'–F') conditions, assuming that $[^{13}C]Dols$ were synthesized solely via the MEP (A, D, A', and D') or the MVA (B, E, B', and E') pathway, or with a contribution of both pathways. Green and blue traces represent the experimental spectra recorded in control and osmotic stress conditions, respectively, while red traces represent the theoretical ones. Vertical lines indicate the calculated m/z of cationic, ammoniated ($[M+NH_4]^+$), sodiated ($[M+Na]^+$), and potassiumated ($[M+K]^+$) forms of monoisotopic $[^{12}C_{75}]Dol-15$ and $[^{12}C_{100}]Dol-20$ ions.

Table II. Number of MEP- and MVA-derived isoprene units in Dol-*n* molecules synthesized in control and stress conditions

Dols were isolated from *Arabidopsis hairy roots* fed [1-¹³C]Glc upon control and stress conditions. n_{MEP} and n_{MVA} stand for the number of MEP- and MVA-derived isoprene units, respectively; $n = n_{\text{MEP}} + n_{\text{MVA}}$. All n_{MEP} values from the estimated ranges shown give almost equivalent models (according to χ^2 test) for each Dol-*n*.

Dol	Control		Sorbitol	
	n_{MEP}	n_{MVA}	n_{MEP}	n_{MVA}
Dol-13	8–9	4–5	9	4
Dol-14	11–12	2–3	14	0
Dol-15	8–11	4–7	15	0
Dol-16	9–10	6–7	14	2
Dol-17	10–11	6–7	13–14	3–4
Dol-18	9–11	7–9	9–11	7–9
Dol-19	8–10	9–11	8–10	9–11
Dol-20	9–10	10–11	10–11	9–10
Dol-21	11–13	8–10	9–10	11–12
Dol-22	10–11	11–12	9–11	11–13
Dol-23	8–11	12–15	10–12	11–13

expected). Efficient labeling in both control and stress conditions was observed for Dol-15 to Dol-17 (Fig. 2 for Dol-15), since only for those Dols were signals corresponding to fully labeled molecules observed at $m/z = M + 2n$, where M is the m/z of sodiated mono-isotopic [¹²C]Dol-*n*, and the relative content of the fully labeled Dol-15 to Dol-17 in the total Dol mixture was increased substantially in stress conditions (Fig. 3). Dol-18 was efficiently labeled only upon osmotic stress, while the longer Dols were not labeled from this precursor.

The observed increased deuterium incorporation to Dol-15 to Dol-17 upon osmotic stress supports the increased contribution of the MEP pathway to their biosynthesis, confirming the results obtained by [1-¹³C]Glc feeding. On the other hand, the divergent labeling of various Dol species again suggests that individual Dol families are synthesized by different CPTs, which are regulated independently and have different access to the DX precursor, possibly due to their sub-compartmentalization.

Labeling with [²H]MVL

This labeling pattern was different from that observed for DX labeling (Figs. 2 and 3; one deuterium atom per isoprene unit is expected). Fully labeled Dol-15 to Dol-18 molecules ($m/z = M + n$) were synthesized in both control and osmotic stress conditions, and [²H]Dol-14 was observed in the control conditions only. This observation suggested that, under these feeding conditions (i.e. in the presence of the exogenous MVL), Dol-15 to Dol-18 originate mostly from the MVA pathway. Interestingly, Dols longer than Dol-18 were only partially labeled, and both the extent of the labeling and the fraction of the labeled molecules decreased with increasing n (Fig. 3). Osmotic stress exacerbated this relationship, supporting the decreased contribution of the MVA pathway in Dol biosynthesis in these

conditions. Moreover, as observed above, osmotic stress induced the synthesis of the dominating Dols (Dol-15 to Dol-17) only.

As shown above, signals corresponding to maximally deuterated Dol-15 to Dol-17 molecules (in accordance with the labeling pattern expected for the applied precursor) were recorded for both precursors in control conditions and stress. It should be noted, however, that feeding specific precursors can alter the regulation of the isoprenoid-generating pathways, and in these conditions, their relative contribution need not reflect the native situation (Lipko and Swiezewska, 2016). Consequently, quantitative elucidations aimed at estimation of the number of MEP- versus MVA-derived isoprene units could not be performed using pathway-specific precursors.

Effect of Sorbitol on the Biosynthesis of Phytosterols

In order to elucidate whether sorbitol affected global isoprenoid metabolism, its effect on the biosynthesis of phytosterols (β -sitosterol, stigmasterol, and campesterol) was analyzed using gas chromatography-mass spectrometry (GC-MS) in addition to the study of Dols. It should be noted that the level of ¹³C labeling of stigmasterol was substantially lower than that of the two remaining sterols.

Sorbitol treatment shifted the isotopic envelopes for all analyzed ¹³C-labeled phytosterols labeled with [U-¹³C₆]Glc (Fig. 8A). Estimation of the ¹³C isotopic enrichment of phytosterols, reflecting the effective ¹³C isotopic abundance of their biosynthetic precursors, was performed as for Dols and revealed $94.5\% \pm 1.3\%$ and $79\% \pm 1.2\%$ for the control and sorbitol-treated roots, respectively. Importantly, similar values of the effective ¹³C isotopic abundance of Glc, $93.9\% \pm 1\%$ versus $80.7\% \pm 1.3\%$, were found based on the isotopic enrichment of [¹³C]Dol labeled with [U-¹³C₆]Glc, confirming the universal nature of the observed metabolic effects of sorbitol.

The values of the effective ¹³C abundance estimated above were further used to calculate the theoretical mass spectra of ¹³C-labeled phytosterols synthesized from [1-¹³C]Glc as the precursor. As for Dol, the theoretical spectra were calculated for all three phytosterols, assuming their exclusive origin from either the MVA or the MEP pathway.

In control conditions, the maximum of the experimental mass spectrum was located between the theoretical envelopes calculated for the MVA and MEP pathways for each phytosterol (Fig. 8A, second left column). This suggested that, in fact, IPP derived from both pathways contributed to phytosterol biosynthesis in the applied experimental model.

Upon sorbitol treatment, the experimental isotopic envelope was shifted to lower m/z values for all phytosterols analyzed, suggesting an increased contribution of the MEP pathway to phytosterol biosynthesis under osmotic stress, since, similar to Dols,

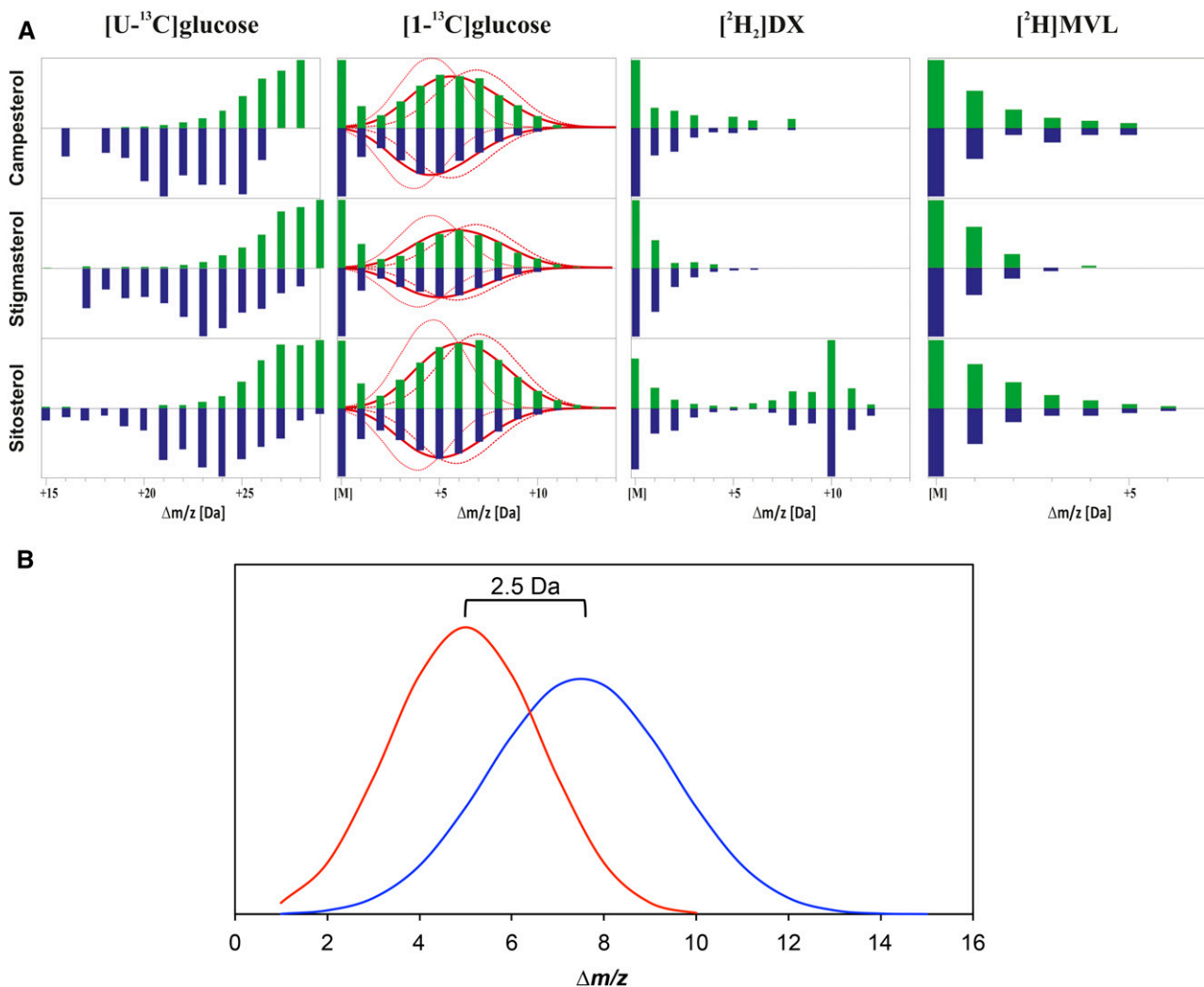


Figure 8. Mass spectra of phytosterols isolated from roots fed various metabolic precursors, $[U-^{13}C_6]$ Glc, $[1-^{13}C]$ Glc, $[^2H_2]$ DX, or $[^2H]$ MVL, in the absence or presence of sorbitol (green or blue bars, respectively). For labeling with $[1-^{13}C]$ Glc, three theoretical isotopic envelopes of the mass spectra are presented for each phytosterol, calculated with the assumption that the phytosterol originates exclusively from either the MEP or the MVA pathway (dotted or dashed lines, respectively) or from both (thick solid lines). Note that the m/z axis is adjusted to the value of the molecular mass of the respective monoisotopic $[^{12}C]$ phytosterol. For consistency, only the fragments of the mass spectra containing signals corresponding to the molecular ions of $[^{13}C]$ phytosterol are presented for labeling with $[U-^{13}C_6]$ Glc. B, Theoretical mass distributions (isotopic envelopes) estimated for phytosterols, synthesized from $[1-^{13}C]$ Glc solely via the MEP or the MVA pathway (red and blue lines, respectively), are represented by binomial distributions with 10 or 15 tries and $P = 0.5$.

the observed shift cannot be explained solely by the apparent decrease of ^{13}C abundance.

A note of caution is due here: the quantitative modeling of the relative contribution of the MEP and MVA pathways to phytosterol biosynthesis using the methodology applied in this report to Dol is of poor reliability. The main reason for this is the fact that only 10 or 15 carbon atoms per molecule of phytosterol can be labeled from $[1-^{13}C]$ Glc via the MEP or the MVA pathway, respectively. Assuming that the ^{13}C enrichment follows a binomial distribution with 10 (MEP) and 15 (MVA) tries with $P = 0.5$, a difference of 2.5 D is obtained between the maxima of the calculated spectra

for the two pathways, while the expected half-width of the isotopic envelopes is 4 and 5 D, respectively, for the MVA and MEP pathways (Fig. 8B). Consequently, such a small difference makes impossible a quantitative estimation of the relative contribution of the two pathways.

To elucidate the effect of pathway-specific precursors on phytosterol biosynthesis, GC-MS analysis of sterols isolated from roots fed $[^2H_2]$ DX or $[^2H]$ MVL was performed (Fig. 8A). Interestingly, the level of deuterium labeling of stigmasterol was lower than that of campesterol, while the labeling of sitosterol was considerably higher. Sorbitol treatment resulted in a modest

decrease of deuterium incorporation from [^2H]MVL (~85%–90% of control for all sterols), while that from [$^2\text{H}_2$]DX was enhanced slightly (~130% and 115% of control for stigmasterol and β -sitosterol; Fig. 8A).

Moreover, while the total content of phytosterols was not affected by sorbitol (Table I), the labeling rate (de novo biosynthesis) of sitosterol was enhanced considerably in contrast to the decreased labeling of stigmasterol (Fig. 8A). In line with this, the proportion among the phytosterols changed. In control conditions, stigmasterol was the dominant species (43.1% of total phytosterol content), while in sorbitol-treated roots, β -sitosterol dominated (49.5% of total).

Taken together, the analysis of metabolically labeled phytosterols suggests that, in the biological system studied, both the MVA and MEP pathways contribute to their biosynthesis. Although phytosterols are usually considered to be exclusively MVA derived, an equal contribution of the MVA and MEP pathways to their biosynthesis already has been reported in *Croton sublyratus* callus culture (De-Eknamkul and Potduang, 2003). While the relative contribution of the MEP and MVA pathways to phytosterol biosynthesis could not be quantitated, it was clear that osmotic stress enhanced the MEP pathway input.

DISCUSSION

In this report, the cooperation of the MEP and MVA pathways was gauged using Dol as a reporter molecule. The key finding is that the increased contribution of the MEP pathway, at the expense of MVA, to Dol biosynthesis observed upon osmotic stress was estimated quantitatively. Moreover, since the biosynthesis of solely one family of Dols (Dol-14 to Dol-17) was affected without modulation of the biosynthetic route of either short-chain (Dol-13) or long-chain ($n > 17$) Dols, it further validates the applied method.

To allow the quantification of MEP- and MVA-derived isoprene units, a novel method involving the numerical modeling of mass spectra of [^{13}C]Dols metabolically labeled with [^{13}C]Glc was established. Based on the biochemistry of isoprenoid biosynthesis and using simple statistical tools, theoretical mass spectra (iterative models) of the labeled Dols were calculated and fitted to the experimentally recorded ones. The two-step protocol involved the application of [$\text{U-}^{13}\text{C}_6$]Glc to estimate the effective ^{13}C abundance and then [$1\text{-}^{13}\text{C}$]Glc to analyze quantitatively the input of the two different routes of IPP synthesis. The first step was essential, since sorbitol affected the cellular metabolism, probably by increasing the release of Glc from native starch (Valentovic et al., 2006; Krasensky and Jonak, 2012) present in the root inoculum. Additionally, sorbitol also might stimulate the activity of the other, apart from glycolysis, catabolic processes utilizing Glc (e.g. the oxidative pentose pathway), and this, in turn, will result in the shuffling of carbon atoms in Glc molecules. Indeed, abiotic

stress was shown to induce the expression of the oxidative pentose phosphate genes (Caretto et al., 2015). The resulting isotopic dilution of the labeled precursor would affect the subsequent calculations, had it not been corrected for. It also should be underlined that externally applied sorbitol does not serve as a carbon source for root metabolism, since its uptake from the medium is low and is decreased even further in the presence of external Glc (Maurel et al., 2004).

The results presented here suggest that a divergent biosynthetic machinery is engaged in the formation of Dol families of different lengths. Consequently, the MEP- and MVA-derived pools of IPP could be used by dedicated CPTs. The changing Dol composition and labeling profiles suggest the involvement of at least three such enzymes in Arabidopsis roots, similar to the two yeast CPTs, Rer2 and Srt1, responsible for the formation of two Dol families in *S. cerevisiae* (Schenk et al., 2001). Furthermore, the observed specific changes of CPT transcript levels in response to osmotic stress could underlie the adjustment of the Dol spectrum to current requirements. This is probably achieved by CPT compartmentalization (Fig. 9), although several aspects of this model remain elusive (e.g. peroxisomal CPT and PPRD, IPP and oligoprenyl diphosphate transporters). Besides plastids and the endoplasmic reticulum, postulated earlier to harbor CPTs (Skorupinska-Tudek et al., 2008), plant peroxisomes also could possess their own CPT, as was observed in mammals and yeast (Ericsson et al., 1992; Skoneczny et al., 2006). Moreover, the existence of the peroxisomal pathway converting MVA to IPP in mammals and plants (Thompson et al., 1987; Simkin et al., 2011) further supports this concept. Still, the type of all-trans-initiator involved in the biosynthesis of Dols in Arabidopsis roots remains enigmatic.

The deduced topological model of Dol biosynthesis (Fig. 9) presents a simplified scenario, presuming that the homogenous polyisoprenoid chain built of IPPs of solely MEP origin is formed in the plastid. Actually, one cannot exclude the possibility that, especially upon stress, longer polyisoprenoid chains, comprising 11 to 12 MEP-derived isoprene units together with a few isoprene units of MVA origin, are formed in this compartment.

The multifamily composition of the Dol mixture together with different sites of their biosynthesis also could indicate different cellular roles of Dols of various length. The dominating homologs, Dol-14 to Dol-17, probably act as cofactors in protein glycosylation in the endoplasmic reticulum, as observed in yeast (Schenk et al., 2001). *N*-Glycans are crucial for plant growth under stress conditions (Strasser, 2016); therefore, reprogramming of the Dol-14 to Dol-17 biosynthetic route could be indispensable for plant homeostasis. Long- and short-chain Dols are possibly not involved in protein glycosylation (Schenk et al., 2001; Surmacz et al., 2014) but instead could act as a shield against ROS or fulfill other as yet unknown functions.

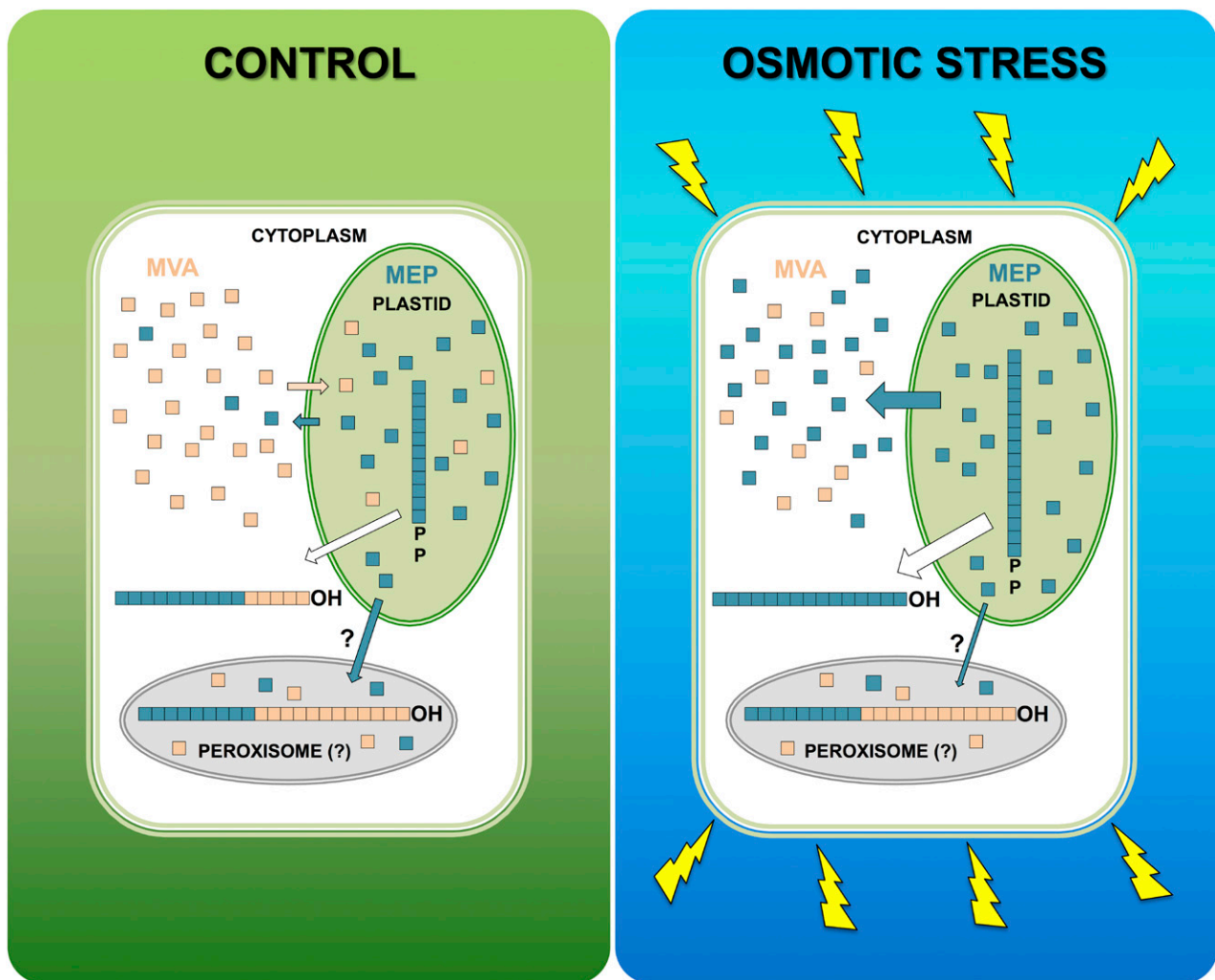


Figure 9. Osmotic stress modulates the input of MEP and MVA pathways to Dol synthesis. The biosynthetic origin of Dol-16 (and other dominating Dols, Dol-14, Dol-15, and Dol-17) changes upon osmotic stress, while that of Dol-21 (and other long-chain Dols, $n > 18$ and also Dol-13) remains unaffected. This implies that, upon osmotic stress, the oligoprenyl precursors synthesized by plastidial CPT and translocated to the cytoplasm are longer than those synthesized in control conditions. In contrast, the synthesis of long-chain Dols proceeds probably in a cellular compartment other than plastids/cytoplasm. Such activity is tentatively assigned to peroxisomal CPT, which probably utilizes an autonomous, MVA-dependent pool of IPP in concert with MEP-derived IPP imported to peroxisomes through plastid-peroxisome contact sites (Shai et al., 2016). Modulation of the intensity of export of plastidial MEP-derived IPP and possibly oligoprenyl diphosphates upon stress is depicted by cyan and white arrows, respectively.

The concomitant modulation of the activity of the MVA and MEP pathways is a subject of extensive studies; the rate of precursor exchange may reach 100% and 80% from the plastids to the cytoplasm and vice versa (Hemmerlin and Bach, 2000; Schuhr et al., 2003), although these values were observed upon inhibitor treatment. Various intermediates (e.g. IPP, DMAPP, GPP, FPP, and oligoprenyl diphosphates; Hemmerlin et al., 2012; May et al., 2013) were shown to be translocated between these compartments. Moreover, a complex bidirectional transfer of precursors was postulated earlier (Skorupinska-Tudek et al., 2008) as well as in the current model (Fig. 9). The observed increased

contribution of the MEP pathway toward Dol biosynthesis upon sorbitol treatment corroborates earlier data suggesting transcriptional stimulation of the MEP pathway by osmotic stress (Wu et al., 2009; Yan et al., 2009) and heavy metals (Ge and Wu, 2005), leading to the accumulation of tanshinone, a diterpenoid, in *Salvia miltiorrhiza* hairy roots. Likewise, osmotic stress, heavy metal salts, and abscisic acid (ABA) treatment increased the accumulation of brachycerine, a monoterpene indole alkaloid, in the leaves of *Psychotria brachyceras* (do Nascimento et al., 2013). Similarly, increased expression of the MEP pathway and carotenoid biogenesis genes was noted in osmotically stressed *Arabidopsis*

roots (Meier et al., 2011). In contrast, the literature data on the effect of osmotic stress on the MVA pathway seem contradictory. Thus, in line with the decreased contribution of the MVA pathway to the biosynthesis of the dominating Dols reported here, a down-regulation of *Brassica juncea* 3-hydroxy-3-methylglutaryl-CoA synthase (the key regulator of the MVA pathway) was observed (Alex et al., 2000; Nagegowda et al., 2005). Conversely, water stress (mimicked by polyethylene glycol treatment) induced both the MVA and MEP pathways and led to an increased accumulation of tanshinone, although MEP seemed to be the main contributor (Yang et al., 2012).

Various mechanisms could underlie the stimulation of the MEP pathway at the expense of MVA upon osmotic stress. First, it could be linked to the cellular energy-saving program, since an enhanced need for ATP is to be expected upon stress and the formation of IPP via the MEP pathway requires less ATP than via the MVA pathway (2 versus 3 mol mol⁻¹ IPP; Gruchattka et al., 2013). Second, it could result from the activation of a sink-like rescue pathway involving the enhanced synthesis of reduced compounds, such as isoprenoids, in order to consume NADPH⁺ overproduced upon stress (Selmar and Kleinwächter, 2013). The consumption of reducing equivalents by the MEP pathway is more efficient than by MVA (3 versus 2 mol of NADPH is used to produce 1 mol of IPP, respectively; Gruchattka et al., 2013). Finally, an enhanced demand for MEP-derived products, such as the antioxidants tocopherols and carotenoids and/or the phytohormone ABA, also could provide the driving force for the induction of this pathway (Abbasi et al., 2007).

The signaling route(s) responsible for the regulation of the MEP/MVA balance remains elusive, although phytohormones should be considered as putative regulators. ABA (synthesized via the MEP pathway) has been found to induce the biosynthesis of MEP-derived metabolites, and both ABA-dependent and -independent signaling pathways appear to be involved in osmotic stress tolerance (Huang et al., 2012). GA₃ has been reported to inhibit the biosynthesis of MEP-derived isoprenoids and to stimulate the MVA pathway (Mansouri et al., 2009). Additionally, ROS also could play the role of such regulators, since their signaling network controls diverse stress responses (Lin and Aarts, 2012). One is also tempted to speculate that methylerythritol cyclodiphosphate, a product of the MEP pathway so far recognized as a retrograde signaling metabolite inducing the expression of selected abiotic stress-responsive genes (Xiao et al., 2012), could be involved. Notably, methylerythritol cyclodiphosphate potentiates the unfolded protein response (Walley et al., 2015) induced upon osmotic stress in plants (Moreno and Orellana, 2011), and interestingly, Dol attenuates this stress reaction (Jozwiak et al., 2015).

In conclusion, Dol is the compound of choice to analyze quantitatively the cooperation of the MEP and MVA pathways, owing to its mixed MEP/MVA origin and the large number of carbon atoms per molecule,

allowing the use of reliable iterative models (e.g. for Dol-16, the number of carbon atoms labeled by [1-¹³C]Glc equals 32 or 48 for the MEP or the MVA pathway, respectively). Furthermore, the occurrence of a complex mixture of Dols in plant tissues (13 homologs in *Arabidopsis* roots) enables cross-validation of the obtained models. Since Dols are a common component of plant roots, application of the experimental approach described here (i.e. metabolic labeling followed by a meta-analysis of Dol mass spectra) seems feasible for other plant species. It should be kept in mind, however, that modulation of the contribution of the MEP and MVA pathways, recorded for Dol biosynthesis, should be interpreted critically. Although Dol might be considered as an indicator, sensing the reprogramming of the isoprenoid generating systems in plants, the input of the MEP-derived precursors, despite the overall increase, might differ quantitatively for particular subclasses of isoprenoids (as observed for different Dol families); this difference might result from a divergent subcellular localization of these compounds.

Moreover, the methodology described in this report is based on metabolic labeling with Glc. Such an approach is clearly applicable to heterotrophically grown tissues/cells, while the feeding of intact plants or detached photosynthetic organs might be more complex for several reasons. First, the uptake of Glc by intact plants might be low, since plants generate their biomass exclusively from CO₂. However, the metabolism of [¹³C]Glc observed in the leaves of aseptically grown intact tobacco (*Nicotiana tabacum*) plants fed [U-¹³C₆]Glc via the root system provided a proof of concept for this labeling method (Ettenhuber et al., 2005), and the applicability of this approach was confirmed later (summarized in Bacher et al., 2016). The incorporation of [¹³C]Glc in these circumstances might be explained by the different biosynthetic origins of the MEP pathway substrates: glyceraldehyde 3-phosphate is derived mostly from photosynthesis, while pyruvate originates from glycolysis (Pokhilko et al., 2015).

Second, the incorporation of [¹³C]Glc together with the concomitant influx of unlabeled precursors derived from photosynthesis/glucogenesis would result in the substantially lower ¹³C enrichment of Dols or Prens. Consequently, a small *m/z* difference between the maxima of the theoretical envelopes calculated for the MEP- and MVA-derived Dol molecules might be expected (e.g. 1 D for Dol-20 labeled from [1-¹³C]Glc of 10% isotopic ¹³C abundance; Supplemental Fig. S5, left). Therefore, the distinction of these pathways would not be reliable. Fortunately, this problem might be partially overcome by feeding with doubly labeled precursor (e.g. [1,6-¹³C₂]Glc; Supplemental Fig. S5, right); in such a case, the expected *m/z* difference is larger (e.g. 2–3 Da) and enables qualitative/semiquantitative depiction of the biosynthetic origin of Dol. Additionally, such an analysis would be much easier, presuming that the spectrum comprises signals of a single cationic form of Dols (likely after technical modifications of the HPLC-MS analysis).

Secondary metabolites, including polyisoprenoids, play important roles in the adaptation of plants to diverse environmental stimuli and in overcoming stress conditions. Numerous studies have been undertaken to dissect the plant metabolic responses to abiotic stresses, which involve intracellular and extracellular signaling, and modification of the cell metabolism (Obata and Fernie, 2012), including modulation of the activity of the MEP and MVA pathways.

This report describes a new approach to studying the cooperation of the MEP and MVA pathways and adds new players (Dols) to the complex network of the plant response to osmotic stress.

MATERIALS AND METHODS

Plant Material and Growth Conditions

In vitro culture of *Arabidopsis thaliana* hairy roots was propagated as described previously (Jozwiak et al., 2013). For metabolic labeling with a general precursor, roots were grown in one-half-strength Murashige and Skoog medium supplemented with either 2% [^{13}C]Glc or 2% [$^{13}\text{C}_6$]Glc used as a sole carbon source. For labeling with pathway-specific precursors, one-half-strength Murashige and Skoog medium was supplemented with 2% Glc (natural ^{13}C abundance) and one of the precursors, either [5- ^2H]MVA (final concentration of 1 mM) or [5,5- $^2\text{H}_2$]DX (final concentration of 0.5 mM). Labeling was performed for 2 weeks (at this time point, Glc concentration was 1.7%) in parallel in the above-described medium (control) or in the same medium supplemented with 300 mM sorbitol. At this sorbitol concentration, Dol accumulation was increased without unfavorable effects on the growth of the hairy root culture.

To elucidate the effect of other stressors on Dol metabolism, one-half-strength Murashige and Skoog medium containing 2% Glc (natural ^{13}C abundance) was supplemented for 2 weeks with various chemicals at the indicated final concentrations: cadmium chloride (25 or 50 μM) or the oxidative agents hydrogen peroxide (1 mM), *tert*-butyl hydroperoxide (0.3 mM), or methyl viologen (1 μM).

Chemicals

All Dol and Pren standards were from the Collection of Polyrenols (Institute of Biochemistry and Biophysics, Polish Academy of Sciences). Standards of phytosterols were from Sigma-Aldrich. D -[1- ^{13}C]Glc and D -[U- $^{13}\text{C}_6$]Glc were from Cambridge Isotope Laboratories. [5- ^2H]MVA and [5,5- $^2\text{H}_2$]DX were synthesized using the protocols published earlier (Keller, 1986; Meyer et al., 2004) with modification: $\text{NaB}[^2\text{H}]_4$ instead of $\text{NaB}[^3\text{H}]_4$ was used as a substrate to prepare labeled MVA. Thin-layer chromatography plates (silica gel and RP-18) and gels for column chromatography (silica gel 60 and Florisil) were from Merck, and organic solvents (HPLC and p.a. grade) were from POCh. Murashige-Skoog Basal Salt Mixture and all other chemicals were purchased from Sigma-Aldrich and were of analytical grade.

Isolation and Purification of Native and Metabolically Labeled Dols, Prens, and Phytosterols

Roots were harvested, rinsed with water, dried with a paper towel, weighed, and homogenized. Dols, Prens, and phytosterols were isolated as described earlier (Jozwiak et al., 2013) with modifications. Briefly, to isolate Dols, unsaponifiable lipids were purified on a silica gel column eluted with hexane containing increasing concentrations of diethyl ether (0%–25%). Fractions containing Dols (according to thin-layer chromatography on a silica gel plate developed in toluene:ethyl acetate [9:1, v/v] and stained in iodine vapors) were combined, evaporated under a stream of nitrogen, dissolved in propan-2-ol, and subjected to HPLC/UV purification. Internal standards (Pren-19, 10 μg ; or cholestanol, 10 μg) were added prior to homogenization only when the content of Dol or phytosterols was to be estimated. Pren (Pren-9, Pren-11 to Pren-23, and Pren-25) and Dol (Dol-15 to Dol-24) mixtures were used as external standards.

HPLC/ESI-MS Analysis of [^{13}C]Dols and [^2H]Dols

Liquid chromatography-MS analysis of polyisoprenoids was performed on an ACQUITY UPLC I-Class Ultra-Performance Liquid Chromatograph (Waters) coupled with the MALDI-Synapt G2-S HDMS mass spectrometer (Waters) equipped with an electrospray ion source and quadrupole time of flight-type mass analyzer. The separation of polyisoprenoid alcohols was carried out using a 100-mm \times 2.1-mm BEH C18 column (Waters). Solvent A was a methanol and water mixture (9:1, v/v) and solvent B was methanol:isopropanol:hexane (2:1:1, v/v/v) combined as follows: from 0% B to 75% B in 10 min, from 75% B to 90% B in 5 min, from 90% B to 100% B in 1 min, 100% B maintained for 4 min, then from 100% B to 0% B in 1 min. The polyisoprenoids were injected in a mixture of methanol:chloroform (1:1, v/v). The liquid chromatography-MS analysis was carried out at a flow rate of 0.4 mL min^{-1} .

Mass spectra of polyisoprenoid alcohols were recorded in the positive ion mode. The desolvation and cone gas was nitrogen. The measurements were performed at a desolvation gas flow of 448 L h^{-1} , a cone gas flow of 76 L h^{-1} , and a nebulizer gas pressure of 4.6 bar. The capillary voltage was set to 3,800 V, and the sampling cone voltage was set to 87 V.

The instrument was controlled and recorded data were processed using the MassLynx V4.1 software package (Waters).

GC-FID-MS Analysis of [^{13}C]Phytosterols and [^2H]Phytosterols

The GC-MS analysis was carried out on an Agilent 7890A gas chromatograph coupled to an Agilent 5975C MS detector under electron-impact ionization (70 eV). The MS scan range was 33 to 500 atomic mass units. The chromatographic column was an HP-5MS UI capillary column (30 m, 0.25 mm, 0.25 μm). The carrier gas was helium at a flow rate of 1 mL min^{-1} . The flame ionization detector gas flow rate was maintained at 30 and 400 mL min^{-1} for hydrogen and air, respectively. Samples were analyzed with the column held at 265°C for 60 min. The injection was performed in the split mode (10:1) at 290°C. The inlet temperature was set at 250°C, while those of the MS transfer line, quadrupole, and ion source were 275°C, 150°C, and 230°C, respectively. The identification of the compounds was achieved by comparison of their mass spectra with the Wiley 9th Ed. and NIST 2008 Library SW (Revision 2010) database (Agilent Technologies) as well as by comparison of retention times with commercially available standards.

GC-FID Analysis of Sugars in Culture Medium

Aliquots of culture medium (25 μL) containing Glc and internal standard (25 μL of 2% Xyl) were placed in a glass vial. Water was evaporated under a stream of nitrogen, and the vial was placed in a desiccator at 30 mbar. After 48 h, pyridine (462 μL), hexamethyldisilazane (92 μL), and chlorotrimethylsilane (46 μL) were added. The firmly closed vial was heated for 30 min at 60°C in a heating block. Products of derivatization were analyzed by GC-FID.

The GC apparatus was as in phytosterol analysis. Nitrogen was used as the carrier gas at an average flow rate of 1.4 mL min^{-1} . Hydrogen and air flow rates were maintained at 30 and 400 mL min^{-1} , respectively. The inlet and detector temperatures were 210°C and 290°C, respectively, and the oven temperature was programmed at 150°C–210°C–275°C with a 2-min hold at 150°C, an increase rate of 6°C min^{-1} to 210°C, and an increase rate of 40°C min^{-1} and a 10-min hold at 275°C.

Analysis of MDA with Thiobarbituric Acid

Hairy roots (0.2 g fresh weight) were homogenized in 4 mL of 0.1% (w/v) TCA on ice. The homogenate was centrifuged at 10,000g for 5 min, and the supernatant was collected. One milliliter of 20% (w/v) TCA containing 0.5% (w/v) thiobarbituric acid was added to a 0.5-mL aliquot of the supernatant. The mixture was kept in a boiling water bath for 30 min and then quickly cooled on ice. After centrifugation at 10,000g for 10 min, the absorbance of the supernatant was measured at 532 and 600 nm. The A_{600} was subtracted from the A_{532} , and the malondialdehyde (MDA) concentration was calculated using its extinction coefficient (155 $\text{mm}^{-1} \text{cm}^{-1}$; Heath and Packer, 1968).

Quantitative PCR Expression Analysis of CPTs and Pren Reductase

Total RNA was isolated and purified using the RNeasy Plant Mini Kit (Qiagen) according to the manufacturer's instructions. RNA concentration and

purity were verified using the NanoDrop 1000 Spectrophotometer (Thermo Scientific). Before cDNA synthesis, RNA was treated with RNase-free DNase I (Thermo Scientific) according to the manufacturer's instructions, and then first-strand cDNA synthesis was carried out with 2 µg of RNA using the SuperScript III First-Strand Synthesis System for reverse transcription-PCR (Invitrogen) and oligo(dT) primers according to the manufacturer's procedure.

CPT or *PPRD2* expression analysis was performed in a total volume of 20 µL of Luminaris Color HiGreen High ROX qPCR Master Mix (Thermo Scientific) using gene-specific primers (Jozwiak et al., 2013, 2015) in the StepOnePlus Real-Time PCR System (Applied Biosystems) according to the manufacturer's instructions.

The cycle threshold was used to determine the relative expression level of a given gene using the $2^{-\Delta\Delta C_t}$ method. The relative expression level of *CPTs* was analyzed after normalization with the *ACTIN2* gene used as the internal reference. Statistical analysis of the quantitative PCR data was performed using one-way ANOVA with Tukey's posthoc test and GraphPad Prism version 5.00 for Windows (GraphPad Software; www.graphpad.com).

Numerical Models

The experimental mass spectrum of Dol was modeled as the sum of theoretical isotopomer distributions of each particular Dol-*n*, native and/or labeled, and in all cases, various cationic adducts (i.e. H⁺, NH₄⁺, Na⁺, K⁺) were considered.

For native (unlabeled) Dol-*n*, its isotopomer distribution, $B(N, p, k)$, was modeled according to the binomial distribution with N trials and $p \approx 1\%$ (corresponding to natural ¹³C abundance) according to Equation 1:

$$B(N, p, k) = \binom{N}{k} \cdot p^k \cdot (1-p)^{(N-k)} \quad (1)$$

where $N = 5 \cdot n$ represents the number of carbon atoms in a Dol-*n* molecule and k is the number of ¹³C atoms incorporated.

The contribution of various cationic adducts was further taken into account as follows:

$$I(N, p, i) = I_H \cdot B(N, p, i) + I_{NH_4} \cdot B(N, p, i-17) + I_{Na} \cdot B(N, p, i-22) + I_K \cdot B(N, p, i-38) \quad (2)$$

where I_i stands for the relative amount of each cationic adduct, i represents the relative increase of its mass in comparison with that of the protonated monoisotopic ¹²C ion ($i = 0$), and $B(N, p, k) = 0$ for $k < 0$.

For labeled Dols extracted from roots grown on [U-¹³C₆]Glc, the theoretical isotopomer distribution was obtained using the same model, but with $p \approx 99\%$ (corresponding to the ¹³C abundance of the precursor Glc declared by the producer). Slight discrepancies in the level of labeling of individual carbon atoms in the precursor [U-¹³C₆]Glc could affect the final labeling probability, but this was not taken into account in the model.

For labeled Dols extracted from roots grown on [1-¹³C]Glc, two classes of models were considered to reflect the two possible routes of their generation: from IPP synthesized exclusively via a single pathway (MEP or MVA) or, alternatively, from a mixed pool of IPP derived through both these pathways. With [1-¹³C]Glc as a precursor, pathway-specific labeling of IPP results in two or three ¹³C atoms incorporated in a MEP- or MVA-derived isoprene unit, respectively, assuming glycolysis as the only source of the intermediates for IPP formation (Lipko and Swiezewska, 2016; Fig. 1B).

In the pure models for a Dol composed of n isoprene units (Dol-*n*), the number of sites possibly enriched in ¹³C atoms upon [1-¹³C]Glc feeding (N) equals $2 \cdot n$ for the MEP pathway and $3 \cdot n$ for the MVA pathway. In both cases, the labeling probability is 1/2, reflecting the metabolic equivalence of C-1 and C-6 atoms of Glc (Skorupinska-Tudek et al., 2008), and the theoretical isotopomer distribution follows Equations 1 and 2.

In the alternative model, assuming a mixed origin of IPP forming a Dol-*n* molecule, n_{MEP} isoprene units originate from the MEP pathway and n_{MVA} units originate from the MVA pathway, and $n = n_{MVA} + n_{MEP}$. Thus, the theoretical isotopomer distribution can be expressed as a formal convolution of two distributions corresponding to the two pathways according to the equation:

$$C(n_{MEP} + n_{MVA}, p, k) = \sum_{j=0}^k \{B(2 \cdot n_{MEP}, p, j) \cdot B(3 \cdot n_{MVA}, p, k-j)\} \quad (3)$$

with contributions of various cationic adducts calculated according to Equation 2, keeping $B(N, p, i) = 0$ for $i < 0$. Note that, for n_{MVA} or $n_{MEP} = 0$, Equation 3 is equivalent to Equation 1.

Modeling Procedure

Appropriate models were fitted to the set of experimental mass spectra using the Marquardt algorithm (Marquardt, 1963) implemented in the GnuPlot program (available at <http://gnuplot.info>). All Dol-*n* spectra were fitted simultaneously by optimization of I_x contributions (Eq. 2, independently for each Dol) and the common value for the ¹³C enrichment (p in Eq. 1 or 3), separately for each experimental condition. In the convolution approach (Eq. 3), for each Dol-*n*, all possible combinations of integer values of n_{MEP} and n_{MVA} were tested to obtain the best fit (in terms of χ^2).

Supplemental Data

The following supplemental materials are available.

Supplemental Figure S1. Effects of cadmium chloride on expression levels of *CPTs* in Arabidopsis hairy roots.

Supplemental Figure S2. Effects of oxidative stress on expression levels of *CPTs* in Arabidopsis hairy roots and level of MDA.

Supplemental Figure S3. Experimental and theoretical spectra of [¹³C]Dol-*n* after feeding [U-¹³C₆]Glc or [1-¹³C]Glc.

Supplemental Figure S4. Estimated number of MVA-derived isoprene units in various Dol-*n* synthesized in control or osmotic stress conditions.

Supplemental Figure S5. Comparison of theoretical mass spectra of Dol-20 calculated for the MEP and MVA pathways obtained from labeling with either [1-¹³C]Glc or [1,6-¹³C₂]Glc of various isotopic ¹³C abundances.

ACKNOWLEDGMENTS

We thank Michel Rohmer (Université de Strasbourg/Centre National de la Recherche Scientifique) and Jolanta Maluszynska (University of Silesia) for stimulating discussions and collaboration.

Received January 12, 2017; accepted April 5, 2017; published April 6, 2017.

LITERATURE CITED

- Abbasi AR, Hajirezaei M, Hofius D, Sonnewald U, Voll LM** (2007) Specific roles of alpha- and gamma-tocopherol in abiotic stress responses of transgenic tobacco. *Plant Physiol* **143**: 1720–1738
- Alex D, Bach TJ, Chye ML** (2000) Expression of *Brassica juncea* 3-hydroxy-3-methylglutaryl CoA synthase is developmentally regulated and stress-responsive. *Plant J* **22**: 415–426
- Bacher A, Chen F, Eisenreich W** (2016) Decoding biosynthetic pathways in plants by pulse-chase strategies using ¹³CO₂ as a universal tracer. *Metabolites* **6**: E21
- Bajda A, Konopka-Postupska D, Krzymowska M, Hennig J, Skorupinska-Tudek K, Surmacz L, Wójcik J, Matysiak Z, Chojnacki T, Skorzynska-Polit E, et al** (2009) Role of polyisoprenoids in tobacco resistance against biotic stresses. *Physiol Plant* **135**: 351–364
- Bergamini E** (2003) Dolichol: an essential part in the antioxidant machinery of cell membranes? *Biogerontology* **4**: 337–339
- Cantagrel V, Lefeber DJ, Ng BG, Guan Z, Silhavy JL, Bielas SL, Lehle L, Hombauer H, Adamowicz M, Swiezewska E, et al** (2010) SRD5A3 is required for converting polyprenol to dolichol and is mutated in a congenital glycosylation disorder. *Cell* **142**: 203–217
- Caretto S, Linsalata V, Colella G, Mita G, Lattanzio V** (2015) Carbon fluxes between primary metabolism and phenolic pathway in plant tissues under stress. *Int J Mol Sci* **16**: 26378–26394
- De-Eknamkul W, Potduang B** (2003) Biosynthesis of beta-sitosterol and stigmaterol in *Croton tigliatus* proceeds via a mixed origin of isoprene units. *Phytochemistry* **62**: 389–398
- do Nascimento NC, Menguier PK, Henriques AT, Fett-Neto AG** (2013) Accumulation of brachycerine, an antioxidant glucosidic indole alkaloid, is induced by abscisic acid, heavy metal, and osmotic stress in leaves of *Psychotria brachyceras*. *Plant Physiol Biochem* **73**: 33–40
- Ericsson J, Appelkvist EL, Thelin A, Chojnacki T, Dallner G** (1992) Isoprenoid biosynthesis in rat liver peroxisomes: characterization of *cis*-prenyltransferase and squalene synthetase. *J Biol Chem* **267**: 18708–18714

- Ettenhuber C, Radykewicz T, Kofer W, Koop HU, Bacher A, Eisenreich W (2005) Metabolic flux analysis in complex isotopolog space: recycling of glucose in tobacco plants. *Phytochemistry* **66**: 323–335
- Ge XC, Wu JY (2005) Tanshinone production and isoprenoid pathways in *Salvia miltiorrhiza* hairy roots induced by Ag⁺ and yeast elicitor. *Plant Sci* **168**: 487–491
- Gruchattka E, Hädicke O, Klamt S, Schütz V, Kayser O (2013) In silico profiling of *Escherichia coli* and *Saccharomyces cerevisiae* as terpenoid factories. *Microb Cell Fact* **12**: 84
- Heath RL, Packer L (1968) Photoperoxidation in isolated chloroplasts. I. Kinetics and stoichiometry of fatty acid peroxidation. *Arch Biochem Biophys* **125**: 189–198
- Hemmerlin A, Bach TJ (2000) Farnesol-induced cell death and stimulation of 3-hydroxy-3-methylglutaryl-coenzyme A reductase activity in tobacco cv Bright Yellow-2 cells. *Plant Physiol* **123**: 1257–1268
- Hemmerlin A, Harwood JL, Bach TJ (2012) A raison d'être for two distinct pathways in the early steps of plant isoprenoid biosynthesis? *Prog Lipid Res* **51**: 95–148
- Huang GT, Ma SL, Bai LP, Zhang L, Ma H, Jia P, Liu J, Zhong M, Guo ZF (2012) Signal transduction during cold, salt, and drought stresses in plants. *Mol Biol Rep* **39**: 969–987
- Jozwiak A, Gutkowska M, Gawarecka K, Surmacz L, Buczkowska A, Lichocka M, Nowakowska J, Swiezewska E (2015) POLYPRENOL REDUCTASE2 deficiency is lethal in *Arabidopsis* due to male sterility. *Plant Cell* **27**: 3336–3353
- Jozwiak A, Ples M, Skorupinska-Tudek K, Kania M, Dydak M, Danikiewicz W, Swiezewska E (2013) Sugar availability modulates polyisoprenoid and phytosterol profiles in *Arabidopsis thaliana* hairy root culture. *Biochim Biophys Acta* **1831**: 438–447
- Keller RK (1986) The mechanism and regulation of dolichyl phosphate biosynthesis in rat liver. *J Biol Chem* **261**: 12053–12059
- Kera K, Takahashi S, Sutoh T, Koyama T, Nakayama T (2012) Identification and characterization of a *cis,trans*-mixed heptaprenyl diphosphate synthase from *Arabidopsis thaliana*. *FEBS J* **279**: 3813–3827
- Krasensky J, Jonak C (2012) Drought, salt, and temperature stress-induced metabolic rearrangements and regulatory networks. *J Exp Bot* **63**: 1593–1608
- Lin YF, Aarts MGM (2012) The molecular mechanism of zinc and cadmium stress response in plants. *Cell Mol Life Sci* **69**: 3187–3206
- Lipko A, Swiezewska E (2016) Isoprenoid generating systems in plants: a handy toolbox how to assess contribution of the mevalonate and methylerythritol phosphate pathways to the biosynthetic process. *Prog Lipid Res* **63**: 70–92
- Mansouri H, Asrar Z, Mehrabani M (2009) Effects of gibberellic acid on primary terpenoids and delta-tetrahydrocannabinol in *Cannabis sativa* at flowering stage. *J Integr Plant Biol* **51**: 553–561
- Marquardt DW (1963) An algorithm for least-squares estimation of non-linear parameters. *J Soc Industr App Math* **11**: 431–441
- Maurel K, Sakr S, Gerbe F, Guillot A, Bonhomme M, Rageau R, Pétel G (2004) Sorbitol uptake is regulated by glucose through the hexokinase pathway in vegetative peach-tree buds. *J Exp Bot* **55**: 879–888
- May B, Lange BM, Wüst M (2013) Biosynthesis of sesquiterpenes in grape berry exocarp of *Vitis vinifera* L.: evidence for a transport of farnesyl diphosphate precursors from plastids to the cytosol. *Phytochemistry* **95**: 135–144
- Meier S, Tzfadia O, Vallabhaneni R, Gehring C, Wurtzel ET (2011) A transcriptional analysis of carotenoid, chlorophyll and plastidial isoprenoid biosynthesis genes during development and osmotic stress responses in *Arabidopsis thaliana*. *BMC Syst Biol* **5**: 77
- Meyer O, Hoefler JF, Grosdemange-Billiard C, Rohmer M (2004) Practical synthesis of 1-deoxy-D-xylulose and 1-deoxy-D-xylulose 5-phosphate allowing deuterium labeling. *Tetrahedron* **60**: 12153–12162
- Moremen KW, Tiemeyer M, Naim AV (2012) Vertebrate protein glycosylation: diversity, synthesis and function. *Nat Rev Mol Cell Biol* **13**: 448–462
- Moreno AA, Orellana A (2011) The physiological role of the unfolded protein response in plants. *Biol Res* **44**: 75–80
- Nagegowda DA, Ramalingam S, Hemmerlin A, Bach TJ, Chye ML (2005) *Brassica juncea* HMG-CoA synthase: localization of mRNA and protein. *Planta* **221**: 844–856
- Obata T, Fernie AR (2012) The use of metabolomics to dissect plant responses to abiotic stresses. *Cell Mol Life Sci* **69**: 3225–3243
- Opitz S, Nes WD, Gershenzon J (2014) Both methylerythritol phosphate and mevalonate pathways contribute to biosynthesis of each of the major isoprenoid classes in young cotton seedlings. *Phytochemistry* **98**: 110–119
- Pokhilko A, Bou-Torrent J, Pulido P, Rodríguez-Concepción M, Ebenhö O (2015) Mathematical modelling of the diurnal regulation of the MEP pathway in *Arabidopsis*. *New Phytol* **206**: 1075–1085
- Pulido P, Perello C, Rodríguez-Concepción M (2012) New insights into plant isoprenoid metabolism. *Mol Plant* **5**: 964–967
- Rohmer M (1999) The discovery of a mevalonate-independent pathway for isoprenoid biosynthesis in bacteria, algae and higher plants. *Nat Prod Rep* **16**: 565–574
- Schenk B, Rush JS, Waechter CJ, Aebi M (2001) An alternative *cis*-isoprenyltransferase activity in yeast that produces polyisoprenols with chain lengths similar to mammalian dolichols. *Glycobiology* **11**: 89–98
- Schuh CA, Radykevich T, Sagner S, Latzel C, Zenk MH, Arigoni D, Bacher A, Rohdich F, Eisenreich W (2003) Quantitative assessment of metabolite flux by NMR spectroscopy: crosstalk between the two isoprenoid biosynthesis pathways in plants. *Phytochem Rev* **2**: 3–16
- Schwarz F, Aebi M (2011) Mechanisms and principles of N-linked protein glycosylation. *Curr Opin Struct Biol* **21**: 576–582
- Selmar D, Kleinwächter M (2013) Stress enhances the synthesis of secondary plant products: the impact of stress-related over-reduction on the accumulation of natural products. *Plant Cell Physiol* **54**: 817–826
- Shai N, Schuldiner M, Zalckvar E (2016) No peroxisome is an island: peroxisome contact sites. *Biochim Biophys Acta* **1863**: 1061–1069
- Sharma R, De Vleeschauwer D, Sharma MK, Ronald PC (2013) Recent advances in dissecting stress-regulatory crosstalk in rice. *Mol Plant* **6**: 250–260
- Simkin AJ, Guirimand G, Papon N, Courdavault V, Thabet I, Ginis O, Bouzid S, Giglioli-Guivarc'h N, Clastre M (2011) Peroxisomal localisation of the final steps of the mevalonic acid pathway in *planta*. *Planta* **234**: 903–914
- Skoneczny M, Kludkiewicz B, Swiezewska E, Szkopinska A (2006) Activity of *Pichia pastoris* alternative *cis*-prenyltransferase is correlated with proliferation of peroxisomes. *Cell Biol Int* **30**: 122–126
- Skorupinska-Tudek K, Bienkowski T, Olszowska K, Furmanowa M, Chojnacki T, Danikiewicz W, Swiezewska E (2003) Divergent pattern of polyisoprenoid alcohols in the tissues of *Coluria geoides*: a new electrospray ionization MS approach. *Lipids* **38**: 981–990
- Skorupinska-Tudek K, Poznanski J, Wojcik J, Bienkowski T, Szostkiewicz I, Zelman-Femiak M, Bajda A, Chojnacki T, Olszowska O, Grunler J, et al (2008) Contribution of the mevalonate and methylerythritol phosphate pathways to the biosynthesis of dolichols in plants. *J Biol Chem* **283**: 21024–21035
- Strasser R (2016) Plant protein glycosylation. *Glycobiology* **26**: 926–939
- Surmacz L, Plochocka D, Kania M, Danikiewicz W, Swiezewska E (2014) *cis*-Prenyltransferase atCPT6 produces a family of very short-chain polyisoprenoids in *planta*. *Biochim Biophys Acta* **1841**: 240–250
- Surmacz L, Swiezewska E (2011) Polyisoprenoids: secondary metabolites or physiologically important superlipids? *Biochem Biophys Res Commun* **407**: 627–632
- Swiezewska E, Danikiewicz W (2005) Polyisoprenoids: structure, biosynthesis and function. *Prog Lipid Res* **44**: 235–258
- Thompson SL, Burrows R, Laub RJ, Krisans SK (1987) Cholesterol synthesis in rat liver peroxisomes: conversion of mevalonic acid to cholesterol. *J Biol Chem* **262**: 17420–17425
- Valentovic P, Luxova M, Kolarovic L, Gasparikova O (2006) Effect of osmotic stress on compatible solutes content, membrane stability and water relations in two maize cultivars. *Plant Soil Environ* **52**: 186–191
- Walley J, Xiao Y, Wang JZ, Baidoo EE, Keasling JD, Shen Z, Briggs SP, Dehesh K (2015) Plastid-produced interorganellar stress signal MEcPP potentiates induction of the unfolded protein response in endoplasmic reticulum. *Proc Natl Acad Sci USA* **112**: 6212–6217
- Wu SJ, Shi M, Wu JY (2009) Cloning and characterization of the 1-deoxy-D-xylulose 5-phosphate reductoisomerase gene for diterpenoid tanshinone biosynthesis in *Salvia miltiorrhiza* (Chinese sage) hairy roots. *Biotechnol Appl Biochem* **52**: 89–95
- Xiao Y, Savchenko T, Baidoo EE, Chehab WE, Hayden DM, Tolstikov V, Corwin JA, Kliebenstein DJ, Keasling JD, Dehesh K (2012) Retrograde signaling by the plastidial metabolite MEcPP regulates expression of nuclear stress-response genes. *Cell* **149**: 1525–1535
- Yan X, Zhang L, Wang J, Liao P, Zhang Y, Zhang R, Kai G (2009) Molecular characterization and expression of 1-deoxy-D-xylulose 5-phosphate reductoisomerase (DXR) gene from *Salvia miltiorrhiza*. *Acta Physiol Plant* **31**: 1015–1022
- Yang D, Du X, Liang X, Han R, Liang Z, Liu Y, Liu F, Zhao J (2012) Different roles of the mevalonate and methylerythritol phosphate pathways in cell growth and tanshinone production of *Salvia miltiorrhiza* hairy roots. *PLoS ONE* **7**: e46797

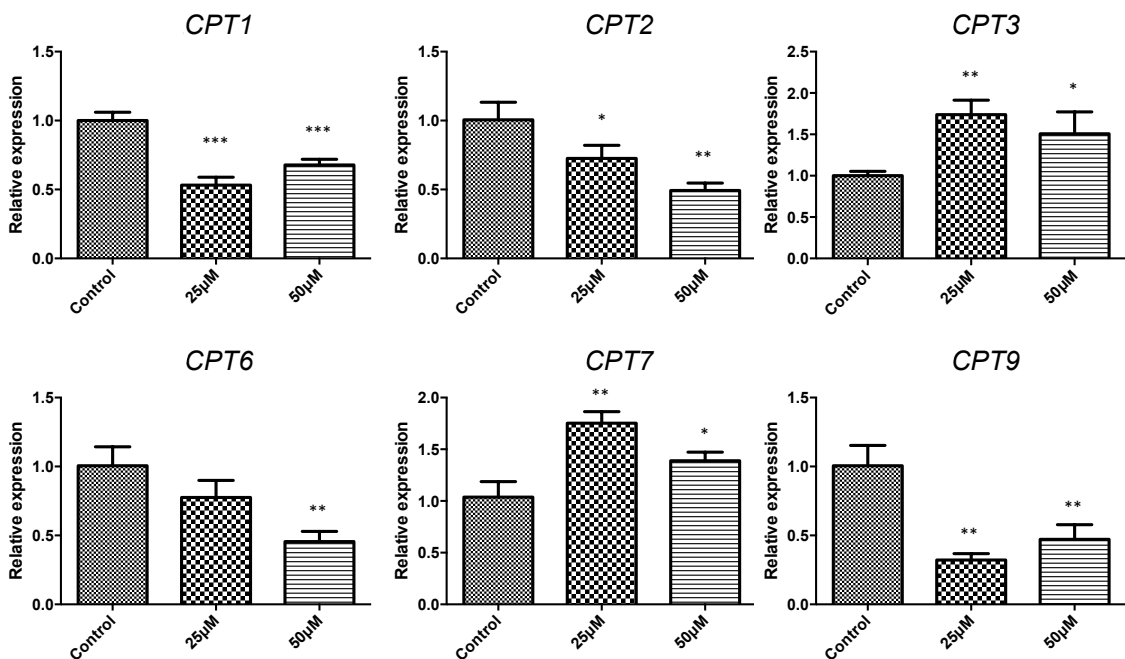
Supplementary Figure 1

Effect of cadmium chloride on dolichol accumulation and expression of CPT-encoding genes

When the hairy root growth medium was supplemented with cadmium salt (25 or 50 μM CdCl_2), dolichol content was moderately increased and reached respectively, 130% and 150% of control (Table 1). Similarly to sorbitol, cadmium salt modulated the composition of the dolichol family and had no statistically significant effect on the accumulation of phytosterols (Table 1).

CdCl_2 decreased the expression of four CPT-encoding genes, *CPT1*, -2, -6 and -9 (to approx. 40% of control) and elevated expression of *CPT3* and -7 (approx. 180% of control for 25 μM CdCl_2). Interestingly, the expression of *CPT6* responds differentially to cadmium ions and sorbitol suggesting a unique role of *CPT6* in the cell response to different environmental stresses.

Cadmium ions have been found to cause disarrangement of actin filaments and Ca^{2+} gradient, thereby inhibiting vesicular trafficking and consequently altering the cell wall organization (Wan and Zhang, 2012). Metabolomic studies on *Arabidopsis* plants treated with a cadmium salt have revealed increased levels of amino acids (alanine, proline, serine), sugars (sucrose, raffinose and trehalose) and other metabolites such as 4-aminobutyric acid and glycerol (Sun et al., 2010). Cadmium salt treatment produced contrasting effects on putrescine level – it was increased in oat and bean plants but decreased, together with spermidine, in the sunflower (Ramakrishna and Ravishankar, 2011). Another well studied group of metabolites affected by cadmium treatment are soluble phenolics, e.g., *p*-coumaric and ferulic acids found to be increased in mycorrhizal roots (Schützendübel and Polle, 2002). In contrast to the present report, cadmium salt treatment caused a significant increase of the concentration of phytosterols - campesterol, β -sitosterol and other isoprenoids such as α -tocopherol (Sun et al., 2010) in *Arabidopsis*. That finding underlines metabolic differences between various biological systems (here, whole plants vs. root culture) even when of a single species.



Supplementary Figure 1

Effect of cadmium chloride on expression level of *CPTs* in *Arabidopsis* hairy roots.

Supplementary Figure 2

Effect of oxidative stress on dolichol accumulation and expression of CPT-encoding genes

Oxidative stress is a common consequence of environmental stressors (Gechev and Hille, 2012) and production of reactive oxygen species (ROS) has been described as a general feature of various rhizotoxic treatments (Zhao et al., 2009). ROS act both as oxidative agents aggressively reacting with cellular components, and as signal transducers regulating plant development, hormone signaling, programmed cell death, and biotic and abiotic stress response and tolerance (Lin and Aarts, 2012).

To gain a deeper insight into the mechanisms responsible for the increased dolichol content upon sorbitol and cadmium salt stresses ROS signaling was mimicked by treating roots with oxidizing compounds – hydrogen peroxide (HP, 1 mM), methyl viologen (MV, 1 μ M) or *tert*-butyl hydroperoxide (*t*BHP, 0.3 mM).

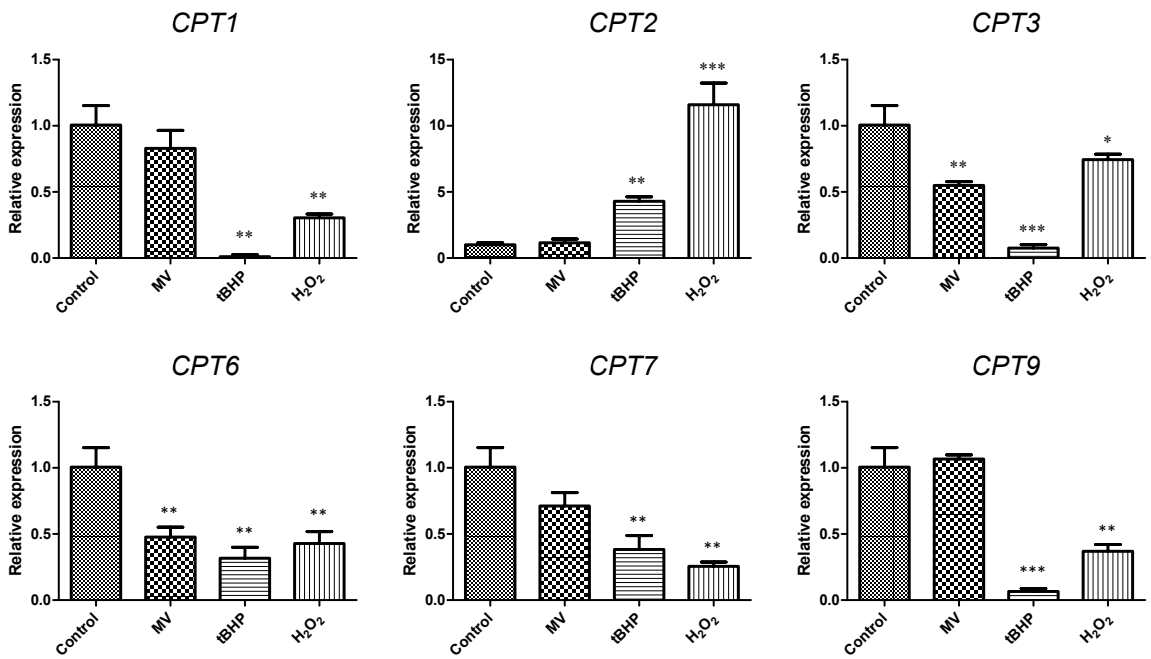
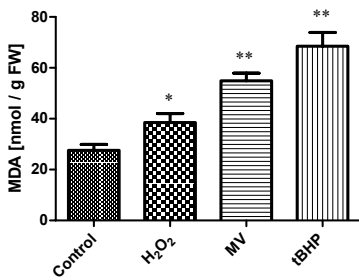
While the HP and *t*BHP treatments resulted in a modest increase of dolichol cellular level (in both cases to approx. 120% of control), MV did not cause a statistically significant change (approx. 90% of control) (Table 1).

In contrast, the sterol content showed profound changes upon *t*BHP and MV treatments, to 260% and 200% of the control, respectively, while HP had no effect (Table 1).

An increased expression of *CPT2* was observed upon the *t*BHP and HP treatment (8- and 12-fold, respectively), and decreased expression of three *CPTs* (*CPT1*, -3 and -9). Methyl viologen slightly decreased the transcript level of all the *CPTs* (Supplementary Fig. 2A).

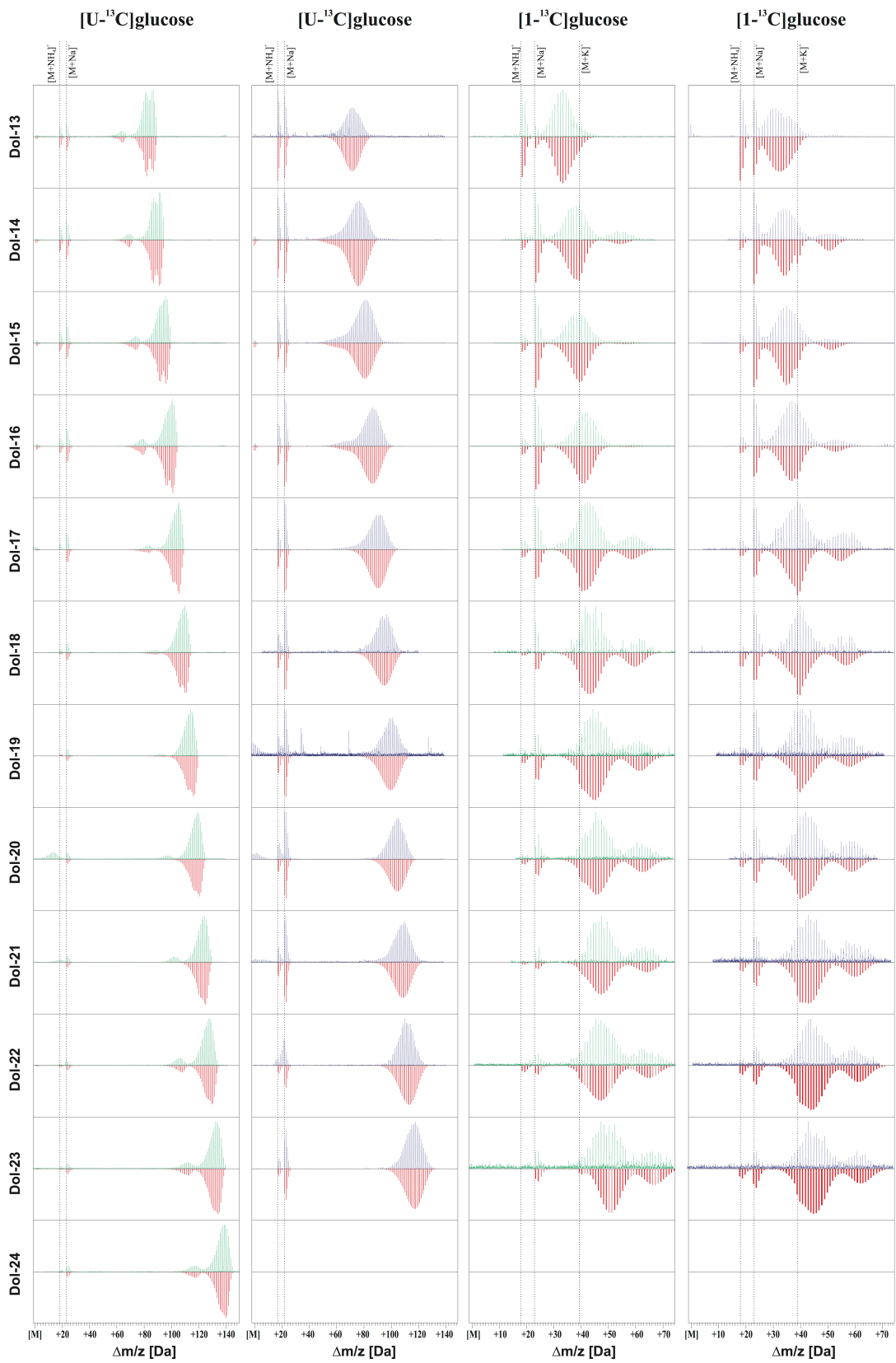
In order to evaluate the oxidative status of the hairy root treated with the oxidizing agents the level of peroxides was followed by measuring the malondialdehyde (MDA) concentration (Supplementary Fig. 2B). All of the stressors tested, *t*BHT, MV and HP, increased the MDA content (to 250%, 200% and 140% of control, respectively).

Thus, at least some of the effects of osmotic and heavy metal stresses on hairy root metabolism investigated in the main body of the present study could be mediated by ROS.

A**B****Supplementary Figure 2**

Effect of oxidative stress on: (A) expression level of *CPTs* in Arabidopsis hairy roots; (B) level of MDA.

Supplementary Figure 3



Supplementary Figure 3

Experimental and theoretical spectra of [^{13}C]Dol-n after feeding [$\text{U-}^{13}\text{C}_6$]glucose (two leftmost columns) or [$1\text{-}^{13}\text{C}$]glucose (two rightmost columns). Theoretical spectra are shown in red, experimental in green (control) or blue (osmotic stress).

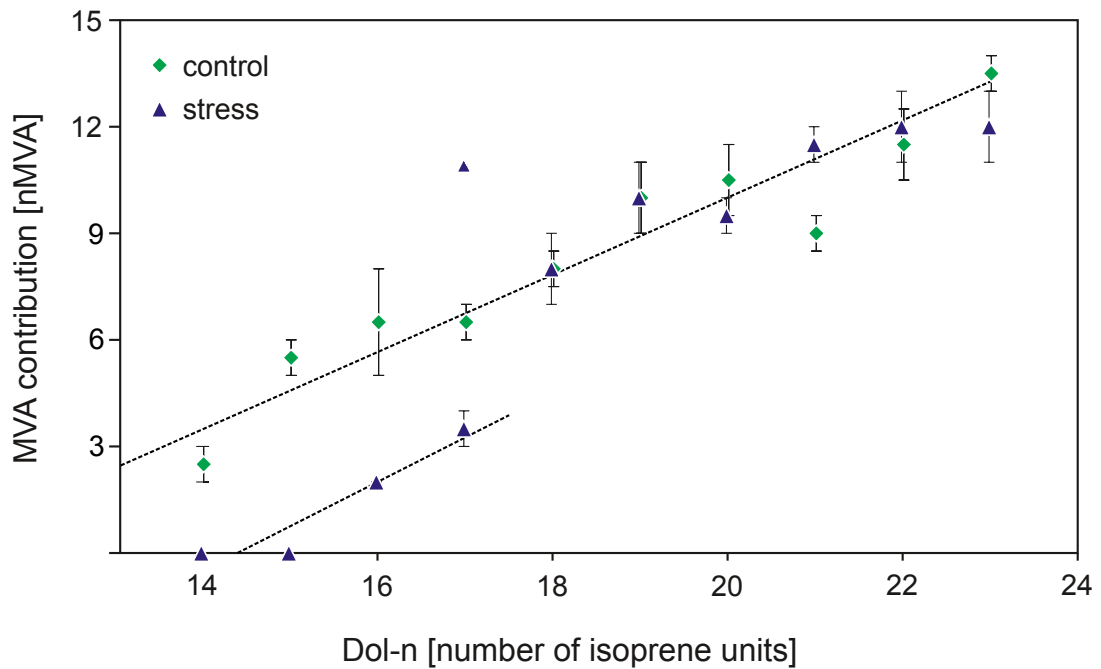
[$\text{U-}^{13}\text{C}_6$]glucose: comparison of the theoretical spectra with experimental ones allowed calculation of the effective ^{13}C abundance of $93.9 \pm 1.0\%$ under control conditions and $80.7 \pm 1.3\%$ under osmotic stress;

[$1\text{-}^{13}\text{C}$]glucose: comparison of the theoretical spectra with experimental ones allowed calculation of the contribution of the MEP and MVA pathways to Dol biosynthesis.

Dotted lines indicate the m/z of ammoniated ($[\text{M}+\text{NH}_4]^+$), sodiated ($[\text{M}+\text{Na}]^+$) and potassiated ($[\text{M}+\text{K}]^+$) ions of monoisotopic [$^{12}\text{C}_{5n}$]Dol-n.

Please note that the m/z axis is adjusted to the value of (M) for each respective Dol-n.

Supplementary Figure 4

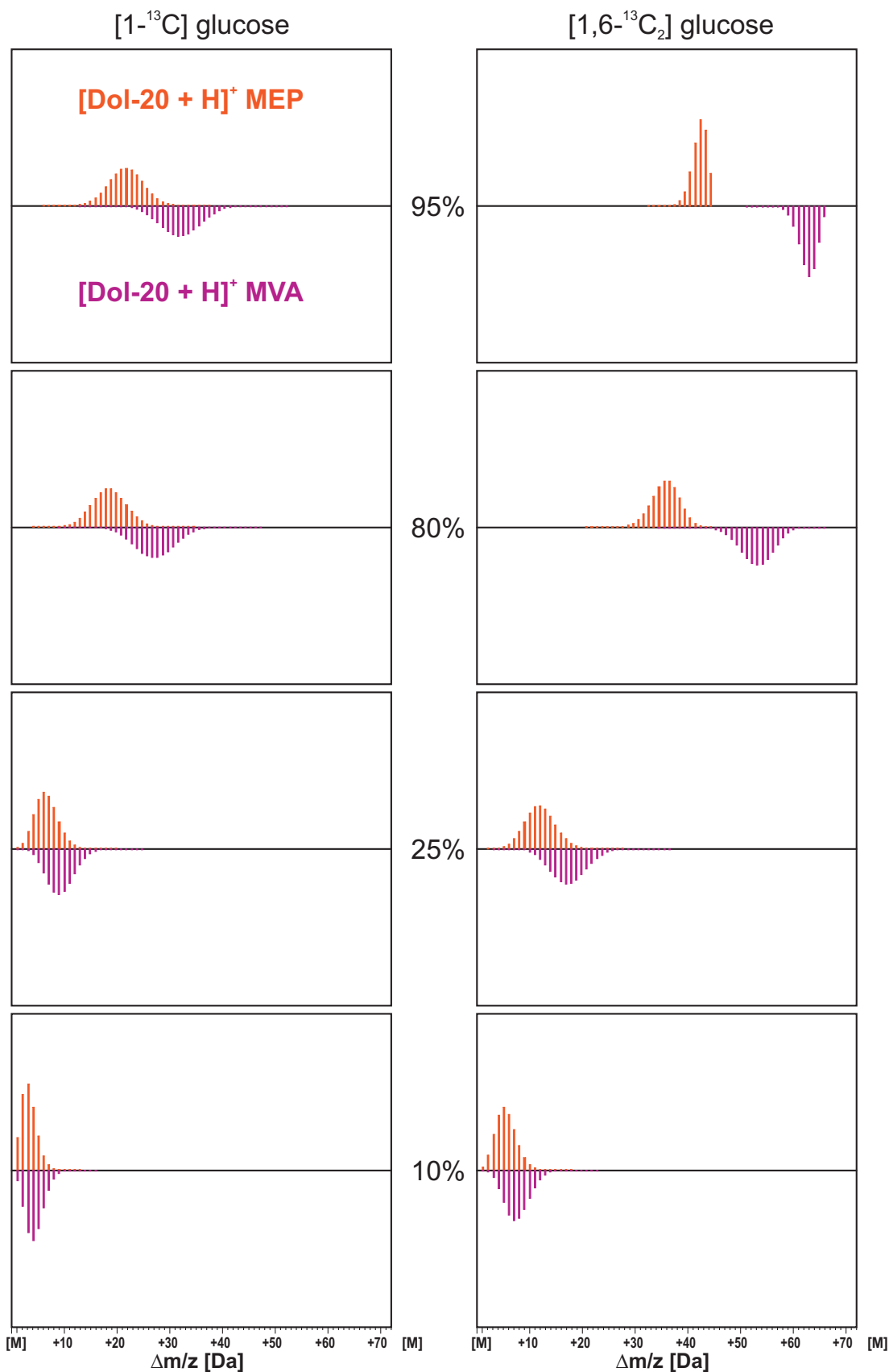


Supplementary Figure 4

Estimated number of MVA-derived isoprene units (i.u.) in various Dol-n synthesized in control (diamonds) or osmotic stress (triangles) conditions (related to Table 2).

Contribution of the MVA pathway to Dol-n biosynthesis is substantially decreased for Dol-14 -17 in the stress conditions. The metabolic origin of longer-chain Dols (Dol-18 – 21) is unaffected by sorbitol.

Supplementary Figure 5



Supplementary Figure 5

Comparison of theoretical mass spectra of Dol-20 calculated for the MEP (orange) and MVA (magenta) pathways obtained from labeling with either $[1-^{13}\text{C}]$ glucose or $[1,6-^{13}\text{C}_2]$ glucose (left and right column, respectively) of various isotopic ^{13}C abundance (95, 80, 25, 10%); shown are protonated $[\text{M}+\text{H}]^+$ ions.

Supplemental references:

Gechev TS, Hille J. 2012. Molecular basis of plant stress. *Cell Mol Life Sci.* **69**:3161-3. doi: 10.1007/s00018-012-1086-2, PMID: 22828863.

Lin YF, Aarts MGM. 2012. The molecular mechanism of zinc and cadmium stress response in plants. *Cell. Mol. Life Sci.* **69**:3187-3206. doi: 10.1007/s00018-012-1089-z, PMID: 22903262.

Ramakrishna A, Ravishankar GA. 2011. Influence of abiotic stress signals on secondary metabolites in plants. *Plant Signal. Behavior* **6**:1720-31. doi: 10.4161/psb.6.11.17613, PMID: 22041989.

Schützendübel A, Polle A. 2002. Plant responses to abiotic stresses: heavy metal-induced oxidative stress and protection by mycorrhization. *J Exp Bot.* **53**:1351-65. PMID: 11997381.

Sun X, Zhang J, Zhang H, Ni Y, Zhang Q, Chen J, Guan Y. 2010. The responses of *Arabidopsis thaliana* to cadmium exposure explored via metabolite profiling. *Chemosphere.* **78**:840-5. doi: 10.1016/j.chemosphere.2009.11.045, PMID: 20044121.

Wan L, Zhang H. 2012. Cadmium toxicity: effects on cytoskeleton, vesicular trafficking and cell wall construction. *Plant Signal Behav.* **7**:345-8. doi: 10.4161/psb.18992, PMID: 22499203.

Zhao CR, Ikka T, Sawaki Y, Kobayashi Y, Suzuki Y, Hibino T, Sato S, Sakurai N, Shibata D, Koyama H. 2009. Comparative transcriptomic characterization of aluminum, sodium chloride, cadmium and copper rhizotoxicities in *Arabidopsis thaliana*. *BMC Plant Biol.* **23**:9-32. doi: 10.1186/1471-2229-9-32, PMID: 19309492.